Energy Conversion and Management: X 23 (2024) 100627

Contents lists available at ScienceDirect

Energy Conversion and Management: X

journal homepage: www.sciencedirect.com/journal/energy-conversion-and-management-x

Advancing Thermal Performance in PCM-Based Energy Storage: A Comparative Study with Fins, Expanded Graphite, and Combined Configurations

Ajay Muraleedharan Nair [a,*], Christopher Wilson [a], Babak Kamkari [b], Jake Locke [c], Ming Jun Huang [a], Philip Griffiths [a], Neil J Hewitt [a]

[a] Centre for Sustainable Technologies, Belfast School of Architecture and Built Environment, Ulster University, BT15 1ED, UK
[b] School of Engineering, Ulster University, BT15 1ED, UK
[c] School of Engineering, University of Warwick, Coventry, CV4 7AL, UK

ARTICLE INFO

Keywords:
Thermal energy storage
Phase change materials
Heat transfer enhancement
Fins
Expanded graphite

ABSTRACT

Phase Change Material (PCM) thermal energy storage systems have emerged as a promising solution for efficient thermal energy storage from low to very high-temperature applications. This paper presents an investigation into the utilization of medium temperature range PCM-based systems for domestic hot water application, focusing on different techniques to overcome the low thermal conductivity of the PCM. Five shell and tube heat exchangers were fabricated employing different heat transfer enhancement methods including fin, expanded graphite (EG), and a combination of fin and EG. The combination of EG and circular fins exhibited the best performance in terms of charging and discharging, maintaining a uniform temperature distribution throughout the system due to extensive conductive network provided by the combination of EG and circular fins. When the PCM/EG/fin heat exchanger system is fully charged, the energy stored in the system is 109% higher than that of the PCM heat exchanger at the same elapsed time. Furthermore, the PCM/EG/fin system demonstrated a faster discharging response compared to other thermal energy storage (TES) configurations, with over 160% higher discharging power than a system without any enhancement methods. These findings emphasize the practical viability of integrating PCM/EG composite materials into thermal energy storage systems, offering a viable solution for meeting high heat demand requirements in domestic hot water applications. Furthermore, the enhanced discharging response observed in the PCM/EG/fin system has significant implications for improving energy efficiency and reducing operational costs in real-world applications.

1. Introduction

An efficient thermal energy storage (TES), is required to bridge the supply and demand of energy for the effective utilization of renewable energies, off-peak electricity price variation and industrial waste heat for building heating applications [12,11,3]. Among the different TES methods, latent heat thermal energy storage (LHTES) using phase change materials (PCM) offers the most flexible operating ranges, comparatively high energy densities and high durability at reasonable costs, which has opened a market for PCM [11–12,30]. However, the inherently lower thermal conductivity of the PCM and associated lower heat transfer characteristics of PCM TES systems must be resolved for the successful commercialization of PCM based energy storage systems. The thermal performance of the PCM TES systems can be enhanced by either design modifications to the heat exchanger (HX) system using various fin configurations, encapsulation of the PCM or by impregnating PCM into highly porous materials such as expanded graphite (EG) or by deploying combinations of these [17,8].

Compared to other forms of TES performance enhancement methods, fins are simple, economical and the most widely used technique for heat transfer enhancement. Various design parameters such as the number of fins, pitch, fin length and fin thickness, have significant influence on heat transfer augmentation [23,19]. The charging and discharging cycle performance of a thermal energy storage system can be greatly enhanced using multiple PCM layers with fins [36]. The multiple PCM layers present higher charging and discharging energy utilisation and the fins enhance the natural convection [18,15]. Agyenim et al. [2]

* Corresponding author.
E-mail address: a.nair@ulster.ac.uk (A. Muraleedharan Nair).

https://doi.org/10.1016/j.ecmx.2024.100627
Received 4 March 2024; Received in revised form 26 April 2024; Accepted 18 May 2024
Available online 19 May 2024
2590-1745/Crown Copyright © 2024 Published by Elsevier Ltd. This is an open access article under the CC BY license (http://creativecommons.org/licenses/by/4.0/).

Nomenclature

ASHP	Air source heat pump
CF	Conventional rectangular fin
Cp	Specific heat
CPCM	Composite PCM
DHW	Domestic hot water
DSC	Differential scanning calorimetry
EG	Expanded graphite
ENG	Expanded natural graphite
FTIR	Fourier transform infrared spectroscopic analysis
HTF	Heat transfer fluid
HX	Heat exchanger
LHTES	Latent heat thermal energy storage
$\dot{m}$	Mass flow rate
MP	Melting point
PCM	Phase change materials
Q	Total thermal energy charged
$\bar{\dot{Q}}$	Time averaged heat transfer rate
$\dot{Q}$ (t)	Instantaneous heat transfer rate
RT	Rubitherm
SS-CPCM	shape selective composite PCM
T	Temperature
t	Time
TES	Thermal energy storage
TOF	Optimised topological fins
T_{PCM}	Average PCM temperature
wt%	Weight percentage

Subscript

in	Inlet
out	Outlet
m	Melting
c	Cooling/solidification

evaluated the thermal performances of a horizontal concentric tube with erythritol as PCM and compared the effect of circular fins and longitudinal fins on the heat transfer performance of the system. The highest heat transfer rate was observed in a longitudinal finned system with reduced subcooling of erythritol during discharging. An extension of this work has been performed by Agyenim and Hewitt [1] by evaluating the suitability of a longitudinally finned horizontal tube-in-tube PCM HX integrated with a heat pump, to utilise cheaper off-peak electricity. Khan and Khan [22,21] experimentally investigated the heat transfer performance of a TES with longitudinal fins. A significant effect on the phase transition rate due to natural convection was observed during charging. The impact of fin length on melting rate is high compared to the thickness and the melting rate increased with the number of tube passes. However, the increase in these parameters resulted in reduced energy storage [24]. Zou et al. [48] studied the effect of various circular fin diameter configurations on the melting and solidification times of RT35 in a vertical cylindrical tube and found that the melting of PCM at the base and at the outer sides was enhanced considerably by increasing the end side fin length. In a similar study Shank et al. [35] experimentally investigated the effect of varying the annular fin width from top bottom on the charging and discharging time of RT55 organic PCM in a concentric tube heat exchanger. Four cases of variable width fins with 4 fins and 8 fins were compared with corresponding four cases of uniform fins. The fin configuration with narrow fin width at the top and wide fin at the bottom presented lowest charging discharging time compared to other configurations. Egea et al. [6] designed a novel concentric tube HX with four sets of scraper blades to remove the solidified PCM layer from the heat transfer fluid (HTF) tube wall to enhance the discharging process. The scraper blade effectively removed solidified PCM layer from the inner wall and the latent heat was completely extracted in a short time compared to the TES unit without the blades. Besides, the heat release rate was two to three times higher than the system without scraper blades. He et al. [13] compared the thermal performance of three LHTES units, one without any fins, second one with conventional rectangular fins (CF) and third one with numerically optimised topological fins (TOF). The charging discharging analysis indicated that the topological fins outperformed both the LHTES units. The heat transfer efficiency of TOF unit was 67.5 % higher than finless unit and 22.8 % higher than CF unit.

Impregnating the PCM into the porous sites of highly conductive matrices to form shape-selective composite PCM (SS-CPCM) is an effective way to enhance the heat transfer performance of the PCM TES systems [25,43]. When PCM is impregnated into the porous matrices, the capillary force of the porous network structure will hold the molten PCM even if it is heated above the melting point (MP) of the PCM [4]. This approach has been widely studied to improve thermal conductivity, supercooling, leakage, and corrosion issues associated with PCM [16]. EG is a potential candidate for composite PCM preparation due to its chemical inertness, high thermal conductivity, mechanical and thermal stability, large porous network, and high specific surface area [33]. Being chemically inert, it is compatible with both organic and inorganic PCM [45]. PCM/EG composites exhibit high thermal stability. Even after a large number of thermal cycles, it retains its thermophysical properties without significant change [34,46]. PCM/EG composites can achieve 10 to 100 times enhancement of the thermal conductivity when a 10 to 30 wt% of EG is used [41,26].

Medrano et al. [27] compared the thermal performances of a simple double pipe HX, double pipe with PCM/EG matrix composite, double pipe with circular fin, compact HX and a small plate HX. The double pipe with PCM/EG matrix had the highest average thermal power compared to the other HX systems. In a similar study, Merlin et al. [28] compared the thermal performance of a concentric tube PCM system with systems employing various heat transfer enhancement methods such as circular fins, graphite powder and expanded natural graphite (ENG) matrix. Compared to the other configurations, the PCM/ENG system exhibited the highest overall heat transfer coefficient value, about 3000 $W \bullet m^{-1} \bullet K^{-1}$. Lin et al. [26] has incorporated PCM/EG composite with double spiral tube heat exchanger and studied the energy storage behaviour of the system for medium high temperature solar energy utilisation. The experimental and numerical results were in good agreement. An experimental comparative study of a conventional shell and tube PCM unit with a PCM/EG composite TES unit was conducted by Yazici et al. [44]. The PCM/EG composite exhibited 35 times higher thermal conductivity than the pure PCM and the total melting time was reduced by 92 % with the use EG. The PCM/EG TES unit was tested without any outer covers and there was no leakage of molten PCM was observed. Sadeghi et al. [31] developed an evacuated tube solar collector with salt hydrate PCM/EG composite in a tankless direct absorption system for solar water heating application. The PCM/EG composite was effective in maintaining the shape stability and the system was effective in storing the thermal energy with less radiative losses. The techno economic analysis of the system showed a payback period of 6 years with an annual CO_2 emission reduction of 5.4 tonnes when it is used to meet 300l of daily hot water. Zheng et al. [47] incorporated PCM/EG composite into a rectangular finned tube heat exchanger and investigated the charging discharging performance of the TES unit under various operating conditions of the HTF. Polyethylene wax/10 wt% EG was used for the study. Due to the high viscosity of the composite, conduction was the major mode of heat transfer and 70 % of the total stored energy was discharged during the discharging process.

In recent years, there has been a surge in research investigating the synergistic potential of PCM and EG in thermal energy storage systems. Various PCM/EG combinations and their thermophysical properties have been studied in detail. Despite this growing body of research, there remains a noticeable gap in the literature regarding the experimental analysis of PCM/EG systems operating within the medium temperature range. Furthermore, studies that explore the various heat transfer enhancement methods during both charging and discharging phases, particularly utilizing a combination of different methods, are sparse.

Thus, this study aims to address these gaps by focusing on the novel aspect of integrating PCM/EG composite based thermal energy storage systems for domestic hot water production application. Our approach involves not only exploring various fin configurations and PCM/EG composites, but also leveraging the unique advantage of using the combination of more than one method of heat transfer enhancement. A combination of PCM/EG/circular fin to augment the heat transfer during the charging and discharging processes proposed. Through rigorous experimentation and comparative analysis with conventional configurations, we aim to unveil the untapped potential of this approach to improve and develop more efficient and sustainable TES solutions.

2. Materials and methods

2.1. Material preparation and characterisation

In order to meet both the EU and UK government guidelines for LHTES domestic hot water production, the melting range of the PCM should be between 50–70 ℃ [5,30]. Therefore, an organic paraffin based PCM (RT55) with a phase transition temperature of 55 ℃ and a latent heat of fusion of 170 kJ/kg was chosen for the study. EG (GFG600 with average particle size of 600 μm) was chosen as a thermal performance enhancer for the organic PCM. EG powder and PCM were mixed at given mass ratios using a melt blend method [38,41]. Twelve different samples of PCM/EG composites were prepared by compressing the mixture in a mould at 40℃ using a hydraulic press to investigate the effect of EG wt.% and packing density on the thermal performance of the composite PCM (CPCM) with different EG compositions (20, 25, and 30 wt%) and compaction densities (800, 900, 1000 and 1050 kg.m^{-3}) Fig. 1. illustrates the materials used for preparing the PCM/EG composite and the physical condition of the material at different stages of the process.

The phase change properties of the PCM such as phase-change temperatures (melting and solidification) and corresponding phase change enthalpies were evaluated using differential scanning calorimetry (DSC- Mettler Toledo DSC1/700). A guarded heat flow meter was used to evaluate the thermal conductivity of the composite block and estimate the thermal conductivity values for different EG compositions and packing densities. The chemical compatibility of both PCM and EG was studied using Fourier transform infrared spectroscopy (FTIR: Varian 640-IR).

The phase change characteristics of PCM and all the three composites with 20 wt%, 25 wt%, and 30 wt% of EG are presented in Fig. 2(a). All the three samples (20 wt%, 25 wt%, and 30 wt% EG/PCM) have the similar DSC curve as that of pure PCM, which indicates that the Paraffin is the major component responsible for the latent heat storage in the composite. The phase change temperatures were not affected much by the presence of EG as reported by Xu et al. [42], whereas the latent heat of fusion and solidification of the pure paraffin decreased with the wt% of EG in the composite samples. The peak melting temperatures of the samples PCM, 20 wt%, 25 wt%, and 30 wt% EG/PCM were between 51.43 °C and 52.23 °C. The key results of the thermophysical property analysis are listed in Table 1. In addition to that, the values of phase change enthalpies obtained from DSC analysis were slightly lower than the theoretical values calculated based on the wt% of PCM in the samples.

The thermal conductivity of pure PCM is 0.2 Wm^{-1} K^{-1} and when it is impregnated into the porous sites of the EG powder and compressed, its thermal conductivity values can be greatly augmented. The effect of different EG wt% and various packed densities on the thermal conductivity of PCM/EG samples are displayed in Fig. 2(b). It is evident that the thermal conductivity increases with EG wt% and packed density. The maximum value of thermal conductivity was observed for a sample with 25 wt% of EG at 1050 kgm^{-3} packing density and which is nearly 4.5 Wm^{-1} K^{-1}, more than 22 times that of pure PCM, showing a very high enhancement in axial thermal conductivity. For 20 wt% EG composites, the enhancement in thermal conductivity with packing density is not that significant compared to 25 wt%. composite. Excess PCM was observed leaking out of the mould when samples were compressed above 1050 kg.m^{-3}, this is attributed to the changes in the microstructure of expanded graphite when it is compressed affecting the capillarity of the PCM.

The FTIR spectra of the RT55/25 wt% EG composite and its components were recorded to study the chemical compatibility of the components and displayed in Fig. 2(c). The absorption peaks of RT55 at 2915 cm^{-1} and 2847 cm^{-1} are attributed to the stretching vibrations of CH_3 and CH_2 groups of RT55. In addition to that, the stretching and rocking vibrations of CH2 caused strong absorption peaks at 1472 cm^{-1} and 729 cm^{-1}. It can be seen from the spectra that the FT-IR spectra of RT55/EG composites have all the peaks of RT55 and EG, i.e., no new peaks were produced by the composite. This indicates that the RT55 and EG are not chemically reacting to form a composite, they are just physically blended, and no new substance has been produced.

2.2. System description

Five different PCM TES units were fabricated and compared for thermal performance during the charging and discharging processes. The TES units consisted of a concentric tube HX, where the annular space was filled with PCM and the HTF passing through the 22 mm

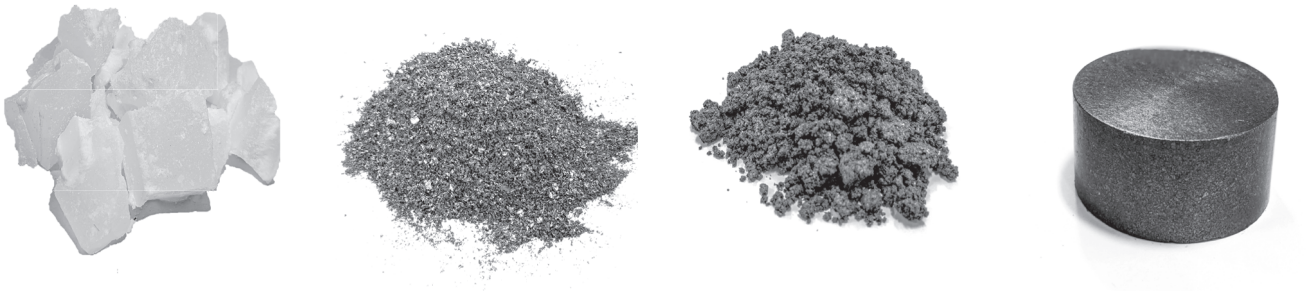


Fig. 1. Images of the materials used for the study and the physical conditions of materials (a) PCM (b) EG (c) PCM EG mixture (d) PCM EG compressed module.

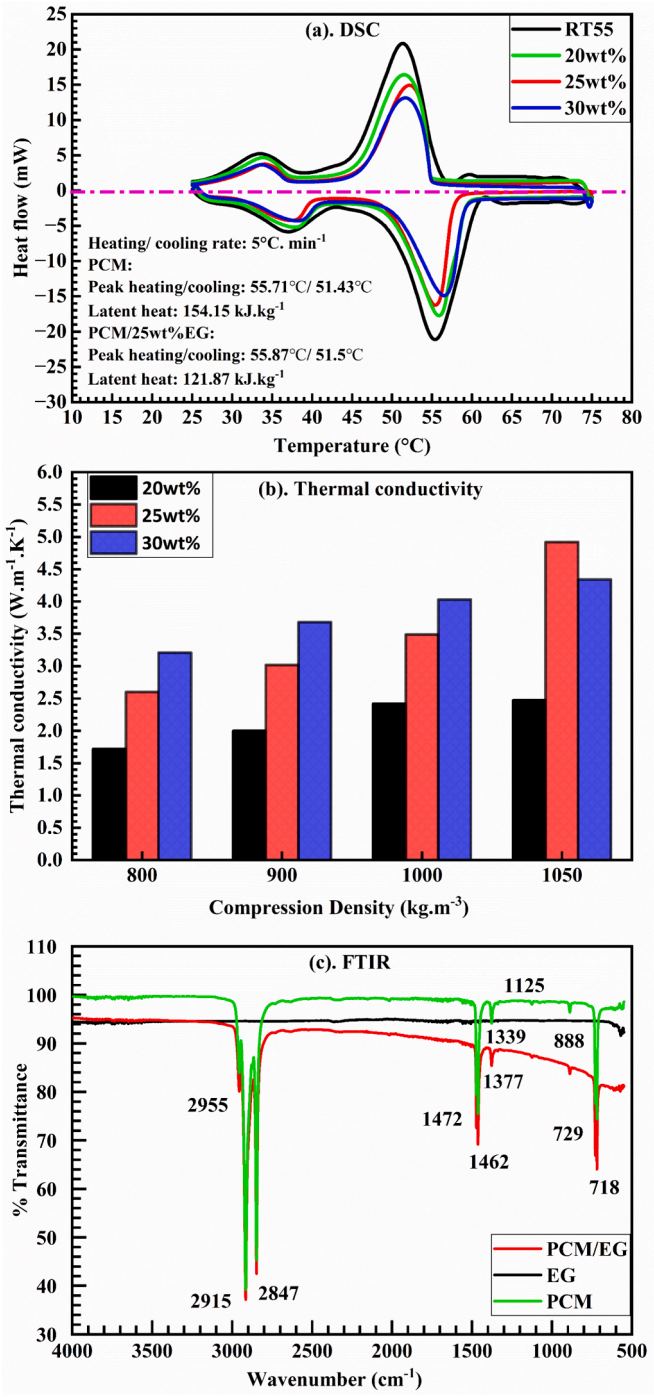


Fig. 2. Thermo-physical property analysis data of the PCM/EG composites (a) DSC curves of the various PCM/EG composites, (b) Thermal conductivity analysis of various PCM/EG samples for different compression densities and (c) FTIR spectra of PCM, EG and PCM/EG samples.

central tube. The first TES unit (PCM HX) was the base reference with no heat transfer enhancement method as shown in Fig. 3a. The second TES unit (PCM longitudinal fin HX) with four fins on the outer wall of the copper tube, as shown in Fig. 3b. The third unit (PCM circular fin HX) had nine circular fins, as in Fig. 3c. In the fourth unit (PCM EG HX) 22 PCM/25 wt% EG modules were stacked in the annular space, which is displayed in Fig. 3d. In the fifth unit (PCM EG fin HX) ten fins of 1 mm thickness and 90 mm diameter were used along with the twenty-two PCM/EG blocks, with two PCM/EG modules between the two fins. Fig. 3e. illustrates the system E fabricated with PCM/EG modules and

Table 1
Results of thermophysical property analysis.

PCM composition	Phase change temperature (°C)	Phase change enthalpy (kJ. kg^{-1})	Thermal conductivity (W. $m^{-1}.K^{-1}$)
RT55	52.28–59.93	154.15	0.2
RT55/20 wt% EG	51.95–59.13	132.35	2.47
RT55/25 wt% EG	52.02–59.06	121.87	4.92
RT55/30 wt% EG	51.91–59.47	114.68	4.34

fins. The major characteristics of all the five LHTES units used in the study are presented in Table 2. Since the quantity of PCM in all the systems is comparable (within 10 % variation), the system performances can be directly compared [9]. Fig. 4. represents the PCM/25 wt% EG composite module used to fabricate the systems D and E. Eight T-type thermocouples (T1-T8) were inserted at locations 15 mm radial from the outer wall of the container into the annular space from bottom to top to record the temperature variation of the PCM during charging and discharging, as shown in Fig. 5.

The PCM storage systems were tested in a facility developed in the university laboratory. Fig. 6. shows the schematic diagram of the test facility used. The charging loop of the test facility consists of a flow meter (FM_1 – Siemens Ultra heat UH50), a thermal bath (2.8 kW), and two PT100 temperature sensors (one each at the inlet (T_1) and outlet (T_2) of the charging circuit of the storage system). While the discharging of the TES unit is performed with mains water. The discharging circuit has a Siemens flow meter (FM_2), and the water temperatures were measured with the same PT100 as in charging loop. A data logger (Data taker DT85) was used to record the flow rates and the temperature readings. Table 3. summarise list all the sensors used with their accuracy values. An infrared thermal imaging camera (Testo 875) was used to record the dynamic temperature distribution of all the systems during charging and recorded the temperature variation of PCM HX, PCM longitudinal fin HX and PCM circular fin HX at every hourly interval and PCM EG HX and PCM EG fin HX every 30 min.

For the charging period analysis, hot water at 70 ℃ was pumped upwards through the copper tube in the storage system at an average flow rate of 2.5 $lmin^{-1}$. The charging continued until all the thermocouples inside the PCM TES units recorded nearly 70 ℃ or 8 h had elapsed. Discharge tests were initiated just after the charging test was over, with mains water at 2.5 $lmin^{-1}$ and continued for one hour. Tap water was used because it had a stable temperature of 15–16 °C sand it's use reflected how a thermal store would heat/preheat water for use in a DHW system.

2.3. Heat transfer calculation method

2.3.1. Heat transfer analysis of the TES units

To evaluate the thermal performance of the LHTES units, instantaneous heat transfer between HTF and PCM, total thermal energy stored/discharged, and the overall thermal powers of the TES units must be calculated from the change in enthalpy of HTF during charging and discharging, respectively.

The instantaneous heat transfer rate between the HTF and PCM during charging and discharging process can be calculated using,

$$\dot{Q}(t) = C_{P,HTF}\dot{m}_{HTF}\,(T_{in}(t) - T_{out}(t)) \quad (1)$$

where $\dot{m}_{HTF}$ is the mass flow rate of the HTF, $C_{p,\,HTF}$ is the specific heat capacity of the HTF, T_{in} and T_{out} are the HTF inlet and outlet temperatures, respectively.

The total energy charged/discharged is calculated by assuming it is equal to the heat lost or gained by the HTF across the storage system,

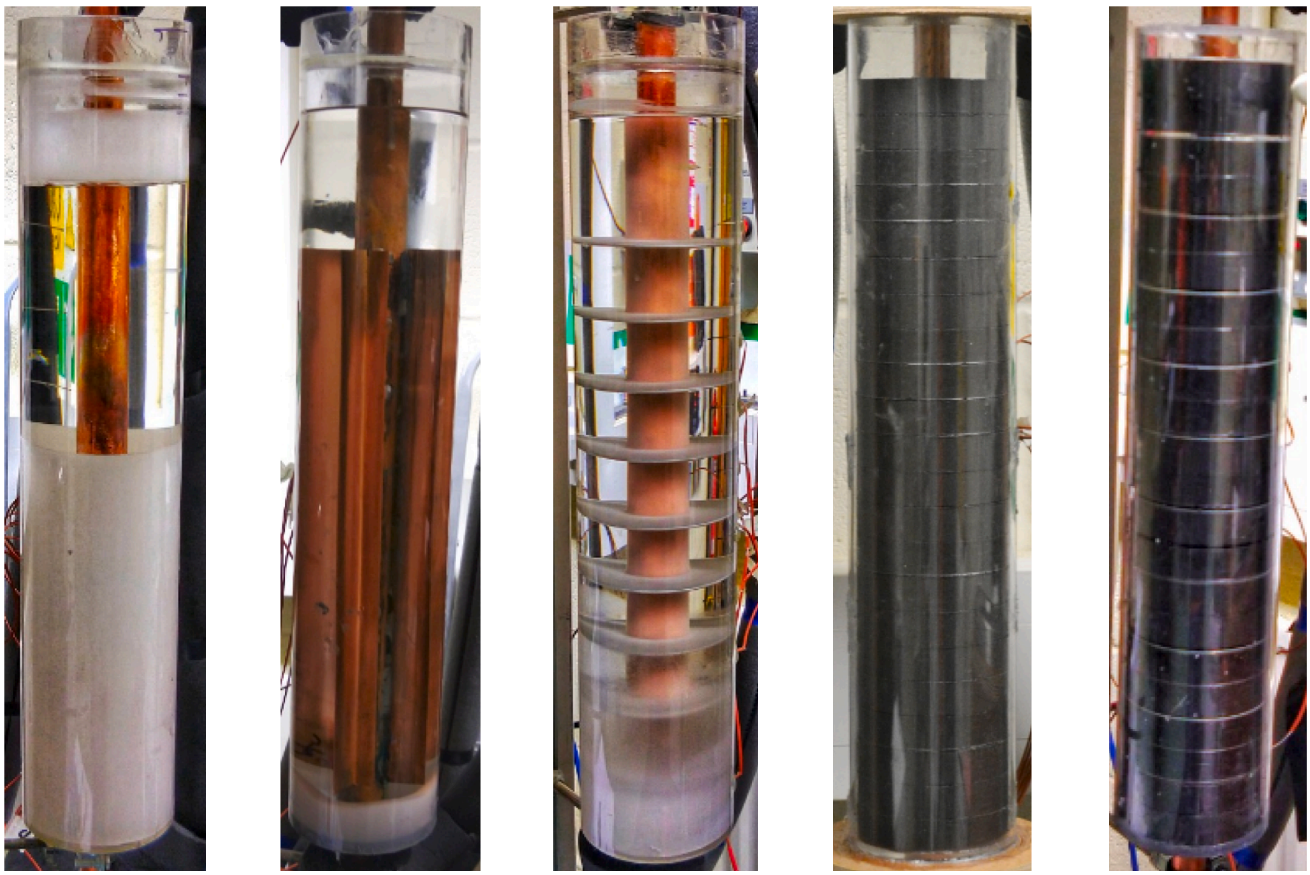


Fig. 3. Images of the PCM storage systems tested during this study. (a) PCM HX (b) PCM longitudinal fin HX (c) PCM circular fin HX (d) PCM EG HX and (e) PCM EG fin HX.

Table 2
Characteristics of PCM thermal energy storage systems studied in this paper.

Parameter	Heat transfer enhancement medium				
	No enhancement	Longitudinal fin	Circular fin	EG	EG/Circular fin
Shell material	Acrylic tube	Acrylic tube	Acrylic tube	Acrylic tube	Acrylic tube
Shell length	500	500	500	500	500
Shell diameter	94	94	94	94	94
Tube material	Copper	Copper	Copper	Copper	Copper
Tube surface	Smooth	Smooth	Smooth	Smooth	Smooth
Tube diameter	22	22	22	22	22
Tube thickness	0.9	0.9	0.9	0.9	0.9
Type of fin	–	Longitudinal	Circular	–	Circular
Fin material	–	Copper	Aluminium	–	Aluminium
Fin length	–	396	–	–	–
Fin width	–	34	–	–	–
Fin diameter	–	–	90	–	90
Fin thickness	–	1	1	–	1
Number of fins	–	4	9	–	10
EG content (wt%)	…..	…..	…..	25	25
Mass of PCM (g)	2387.45	2317.70	2321.80	2256.15	2256.15

neglecting the heat loss from the system and can be calculated using the following equation [14,40]

$$Q_{stored/discharged}(t) = \int_0^t \dot{Q}(t)\,dt \quad (2)$$

The time-averaged heat transfer rate over the melting time ($\overline{\dot{Q}}(t)$), is calculated for different HXs by using the following equations:

$$\overline{\dot{Q}}(t) = \frac{1}{t_{total}} \int_0^{t_{total}} \dot{Q}(t)dt \quad (3)$$

where, t_{total} is the total melting or solidification time of the PCM.

Energy discharge ratio is a useful parameter to evaluate the discharging performance of the PCM TES units, which is calculated as the ratio of thermal energy discharged to the total thermal energy trans-



Fig. 4. PCM/25 wt%EG module having 1050 kg•m^{-3} density, with the 22 mm central hole for the HTF tube.

ferred into the system during charging as shown in the following equation,

$$\text{Energy discharging ratio} = \frac{\text{Qdischarged}}{\text{Qstored}} * 100 \quad (4)$$

The heat transfer enhancement ratio during charging and discharging is another significant factor to quantify the HX thermal performance. Heat transfer enhancement is calculated as the ratio of time-averaged heat transfer rate in the finned HX (radial, circular, PCM/EG or PCM/EG/fin) to that of the HX with no enhancement expressed by the following equation.

$$\text{Heat transfer enhancement ratio} = \frac{\overline{\dot{Q}_{\text{with enhancement}}}}{\overline{\dot{Q}_{\text{no enhancement}}}} \quad (5)$$

where $\overline{\dot{Q}_{\text{with enhancemnt}}}$ and $\overline{\dot{Q}_{\text{no enhancement}}}$ represent the time-averaged heat transfer rates from the HX with enhancement methods and HX with no enhancement, respectively.

The heat loss from the TES units during the process was calculated based on Eq.6 [29]. Heat loss from the system is minimum when the PCM temperature is closer to room temperature, and it increases as the PCM temperature increases. When the system is fully charged, the system presents a constant heat transfer rate, which is equal to the heat loss to the surroundings.

$$\dot{Q}_{\text{loss}} = \frac{\dot{Q}_{\text{final}}}{\left(T_{\text{PCM}_{\text{final}}} - T_{\text{amb}}\right)} \left(T_{\text{PCM}} - T_{\text{amb}}\right) \quad (6)$$

where, $\dot{Q}_{\text{loss}}$ is the heat loss at every time steps, $\dot{Q}_{\text{final}}$ represents the final heat transfer rate to the PCM when the system is fully charged, $T_{\text{PCM}_{\text{final}}}$ is the average PCM temperature when the system is fully charged, T_{PCM} is the average PCM temperature at every time steps and T_{amb} is the ambient temperature. The maximum heat loss from the PCM HX, PCM longitudinal fin HX, PCM circular fin HX, PCM/EG HX and PCM/EG fin HX were 30.33 W, 26.89 W, 23.85 W, 19.08 W and 15.33 W respectively.

2.3.2. Uncertainty analysis

The uncertainty of a variable Y that cannot be measured directly using sensors was determined using Eq. 7 [32] where Ux is the individual uncertainties associated with variable X. The uncertainties were

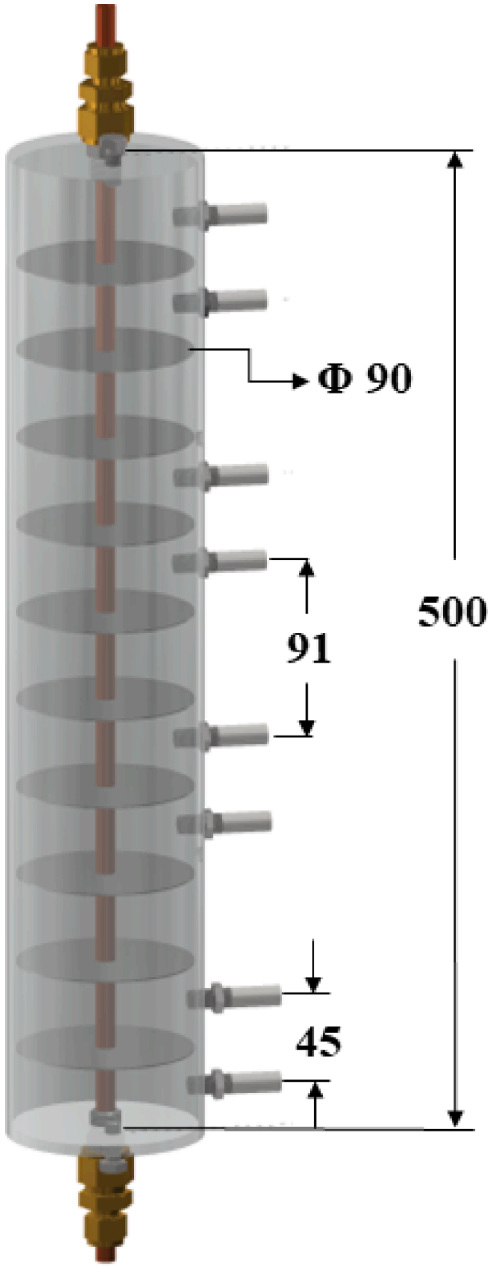


Fig. 5. The position of thermocouples in the LHTES unit.

calculated using the uncertainty propagation function in the EES platform.

$$U_Y = \sqrt{\sum_i \left(\frac{\partial Y}{\partial X_i}\right)^2 {U_{X_i}}^2} \quad (7)$$

By applying Eq. (7) and the uncertainty values sensors listed in Table 3. on Eq. (1) and Eq. (2), the uncertainties of heat transfer rates during charging and discharging of all the five TES units were calculated. The maximum uncertainties of heat transfer rate during both charging and discharging are ± 5.3 % and ± 6.8 % respectively.

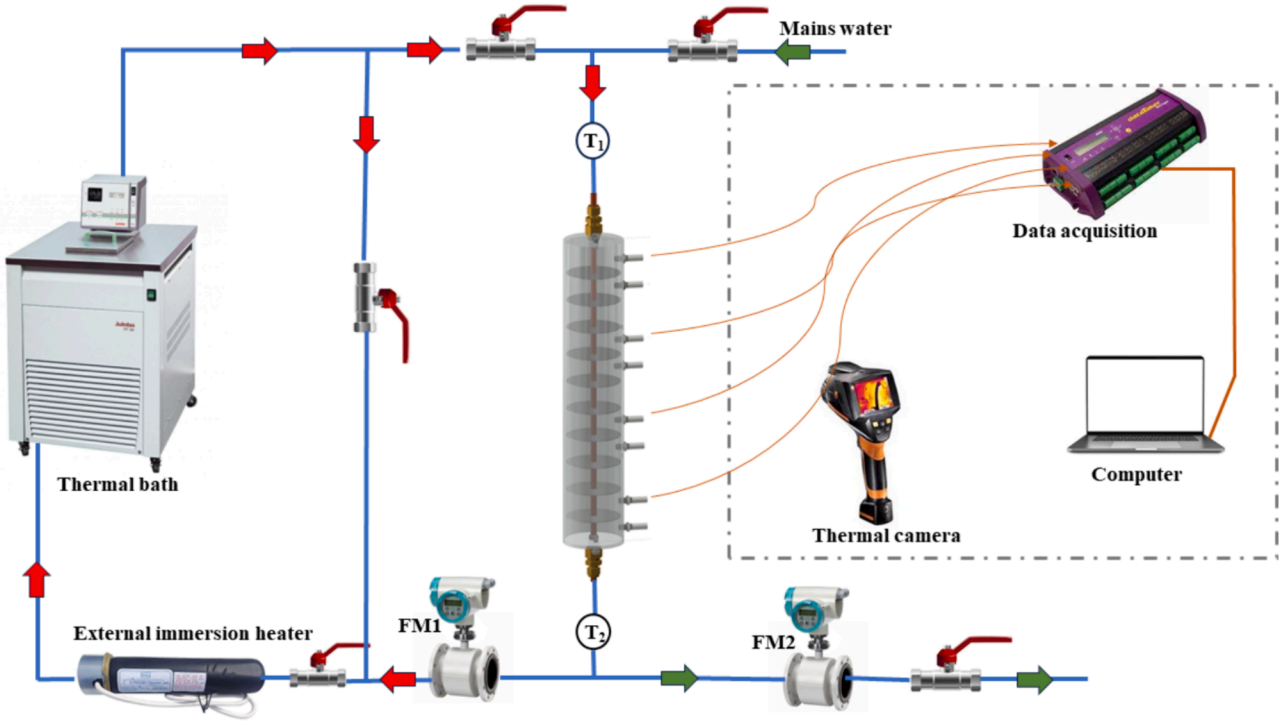


Fig. 6. Schematic diagram of the test facility developed to test the PCM thermal storage systems, where T1 and T2 are the temperature sensors (PT100), FM1, FM2 are the flow meters to measure the HTF temperatures and mass flow rates at the inlet and outlet of the TES unit.

Table 3
Sensors used for measurement and data acquisition.

Sensor	Model	Variable	Range	Accuracy
PT100	Class A type	Temperature (°C)	−50 to 250	± 0.15 °C
Flow meter	Siemens Ultra heat UH50	Flow rate (m^3/h)	0.025 to 5	± 2 %
Thermocouples	T-type	Temperature (°C)	−200 to 200	± 0.1 %
Datalogger	DT85 Datalogger	–	–	–

3. Result and discussion

3.1. Charging period analysis

3.1.1. Charging characteristics

Dynamic temperature variation of the PCM is required to understand the heat transfer mechanism and overall melting behaviour of the PCM, and to calculate the instantaneous thermal power during the process. Fig. 7a-e presents the charging characteristics of the PCM HX, PCM longitudinal fin HX, PCM circular fin HX, PCM/EG HX and PCM/EG/fin HX systems respectively. The red dotted line at 51℃ and 57℃ divides the entire melting regime into three zones. Zone1 represents the solid sensible heating region, Zone2 represents phase change region and Zone3 represents the liquid sensible heating region. As the heat transfers from the HTF to PCM, the PCM temperature rises gradually, and phase change process commences at the melting point. Phase change process can be noticed by the sudden rise in temperature of the PCM.

From Fig. 7a. it is evident that the PCM in the same vertical line of PCM HX has almost same rate of temperature rise. This is an indication of the conduction dominated heat transfer during the earlier stages of charging. Though the initial rate of increase in temperature was slow, there is a sharp rise in T6-T8 at around 60–70 min of charging (vertical black dotted line) is attributed to the strong convection current. This sudden rise in temperature indirectly indicates the formation of the melt front at the top regions of the HX. As the hot water passes from the bottom to the top, the PCM layer close to the copper pipe starts melting and rising to the top due to the density difference between solid and liquid PCM forming a liquid PCM layer at the top. This implies that the heat transfer rate of the top layer of PCM is significantly enhanced due to the circulating convection current and as a result the solid PCM layer close to the liquid solid PCM boundary starts melting at a faster rate compared to the PCM layers in the lower regions of the HX. Similar observations were also reported by Karami and Kamkari [20]. Strong heat stratification is evident from the non-uniform temperature distribution from top to bottom, which is visible in Fig. 7a. This is attributable to the poor heat transfer kinetics offered by the very low thermal conductivity of the organic PCM.

Fig. 7(b) presents the temperature history of the PCM in the PCM longitudinal fin HX system. For the first 50 min of charging, there was a uniform rise in temperature from bottom to top layer of PCM due to the conduction dominated heat transfer. However, temperature of the PCM at the top layer showed an abrupt increase and went above the phase change region in a short time indicating the presence of strong convection current. As can be observed, all the thermocouple readings were above the phase change region in less than five hours of charging. Radial fins exhibited a much higher heat transfer rate than PCM HX due to the extended heat transfer surface along with the strong convection current. Khan and Khan [22] achieved a similar result in their study with longitudinal fins. Whereas the PCM circular fin HX exhibited a uniform temperature distribution from bottom to top throughout the charging process except the lower region near the thermocouple T1 compared to systems A and B, as shown in Fig. 7(c). However, melting commenced slightly earlier at the top layer close to the T8 and T7 thermocouples. This is due to the active convection current passing through the small gap between the edges of the circular fins and the inner wall of the container. A similar observations were made by Karami and Kamkari [20] in an experimental study with solid circular fins. The circular fin configuration exhibited a higher temperature rise throughout the charging process compared to PCM HX and the PCM longitudinal HX, indicating a higher heat transfer rate. The sandwiching effect of the two

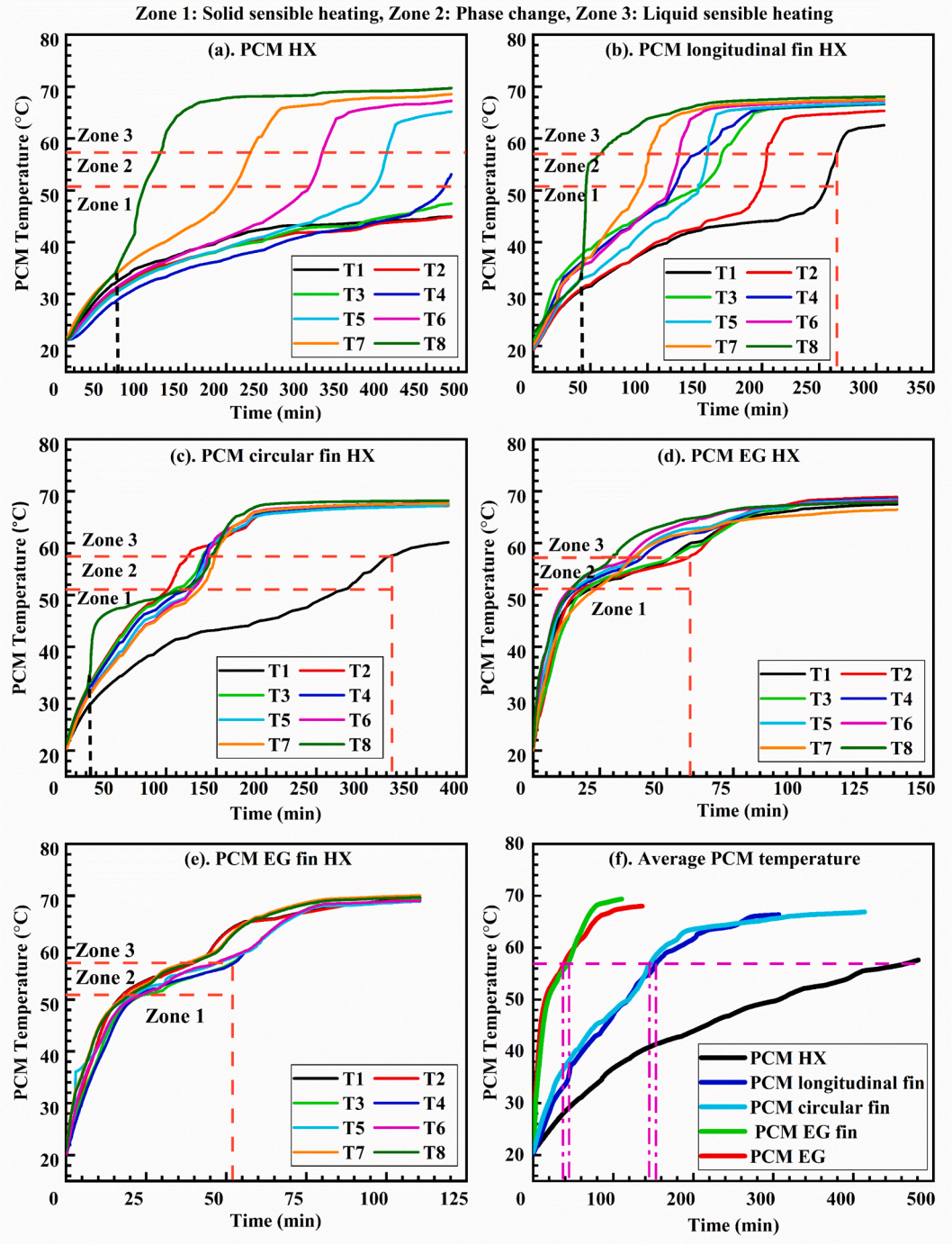


Fig. 7. Transient temperature distribution of the TES systems tested at an HTF inlet temperature of 70°C and 2.6 l.min^{-1}.

circular fins above and below the PCM layers along with the slight convection current resulted in a uniform temperature rise and slightly higher rate of temperature rise compared to the PCM longitudinal fin HX.

PCM/EG HX shown in Fig. 7(d) presented a better uniform temperature distribution and faster heat transfer rates throughout the charging process compared to the first three systems. The rate of temperature rise was higher during the initial period of charging due to the high temperature gradient between the PCM and the HTF. All the thermocouple readings exceeded the peak melting point region in less than 60 min of charging. This is due to the wide heat transfer network structure provided by the expanded graphite. Contrary to systems A, B, and C, conduction is the major mode of heat transfer in system D as the PCM is embedded into the micropores of EG. Similar explanations are valid for the charging characteristics of PCM/EG/fin HX (Fig. 7(e)). However, the rate of increase in PCM temperature was higher and more uniform than in PCM/EG HX. PCM/EG/fin HX exhibited a clear phase change zone ranging over 30 min compared to all other PCM heat exchangers investigated in this study. PCM/EG/fin HX presented the combined effect of EG and circular fin combination.

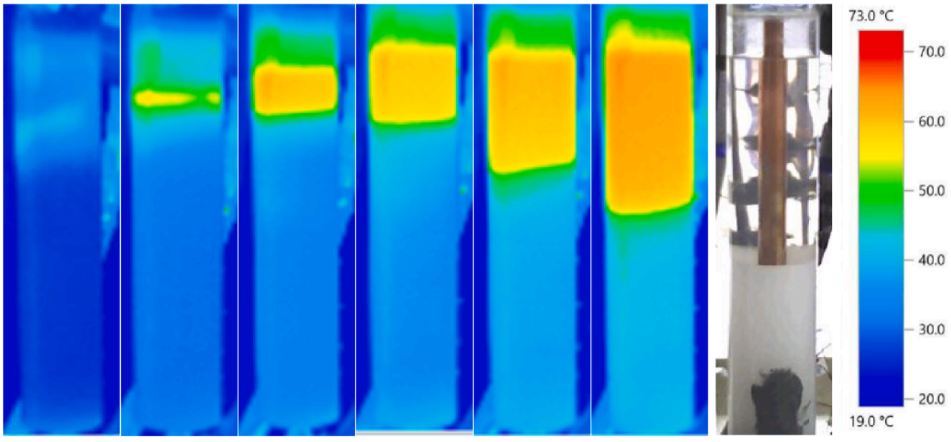
Fig. 7f shows the variation of average PCM temperature during the charging cycle for all the five storage systems. All the enhancement methods have a significant effect on the melting rate of the PCM. The melting of PCM in PCM circular fin HX was 2.8 times faster and 2.5 times faster in PCM longitudinal fin HX compared to the PCM HX system. Whereas PCM/EG and PCM/EG/fin HX exhibited more than eight times

faster melting than PCM HX when the average PCM temperature is compared. The PCM/EG/Al fin system completed charging in 30 % less time than PCM/EG HX. This is a clear indication of the high rate of heat transfer augmentation with the EG-circular fin combination.

3.2.2. Thermal image visualisation of charging

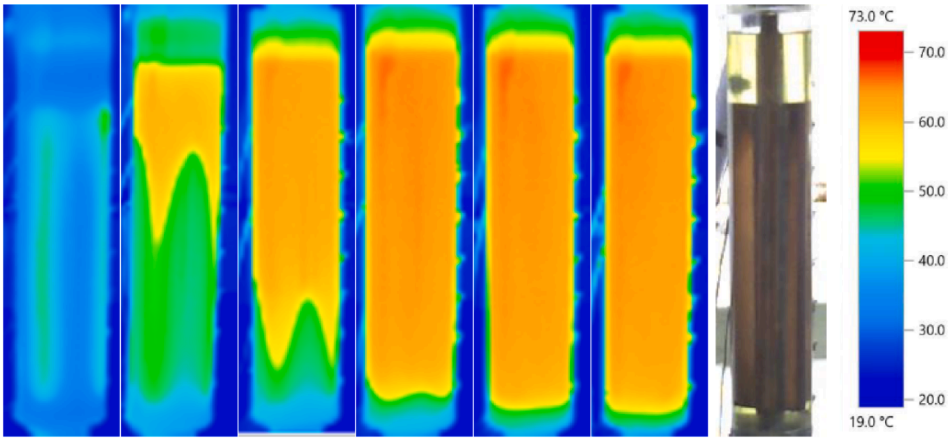
The thermal images in Fig. 8(i-v) compare the dynamic temperature evolution and further explain the evolution of the energy storage in the PCM HX, PCM longitudinal fin HX, PCM circular fin HX, PCM/EG HX and PCM/EG/fin HX respectively. As can be seen in the Fig. 8(i), the temperature of the PCM from bottom to top layer during the first hour of charging was uniform, indicating the conduction dominated heat transfer. As the process continued, a layer of molten PCM was formed at the top of the PCM column during the next hour of charging as a result of the melting of PCM around the copper tube. As the PCM around the copper tube melts and the buoyant force of the liquid PCM exceeds the viscous force, the natural convection current dominates and forms a strong melt front at the top. At the end of 2 h of charging the top layer reached 56.7 ℃ whereas the bottom was at 31℃. As the charging progressed, the melt front moved slowly downwards and occupied only about 55 % of the total PCM even after 6 h with a high rate of stratification from top to bottom indicating very slow heat transfer kinetics offered by the PCM.

The impact of the longitudinal fins on the charging rates of organic PCM is evident in the thermal images of PCM longitudinal fin HX as shown in Fig. 8(ii). During the first hour of charging, temperature of the PCM along the longitudinal fin increased significantly compared to the rest of the area. During the next hour, the melted PCM around the copper tube and the radial fins, rose to the top and this liquid PCM regime occupied 30 % of the total volume forming a strong liquid to solid interface. This is attributed to the strong convection current due to the enhanced heat transfer area provided by the radial fins. The hot liquid interface of the melt front enhanced the heat transfer rate and the melt front started occupying more regions downwards at a faster rate. As a result, around 70 % of the total PCM was at an average temperature of 58℃ and more than 80 % at the end of 4 h of charging with an average PCM temperature of 62.2℃. At the end of 6 h of charging only a small amount of PCM in the bottom zone remained solid. The PCM circular fin HX exhibited a more uniform temperature evolution from top to bottom as evident in Fig. 8(iii). The fins divided the annulus into small enclosures and natural convection formed between the two fins resulted in more uniform charging from bottom to top compared to the first two HXs. With the sandwiching effect of fins, heat transferred radially from the copper pipe was significantly improved, which along with the natural convection resulted in high heat transfer rate compared to PCM HX and PCM longitudinal fin HX. However, the effect of natural convection was weaker in PCM circular fin HX compared to the first two HXs as the circular fin hinders the upward convection flow. More than 70 % of the



(a). 1h (b). 2h (c). 3h (d). 4h (e). 5h (f). 6h

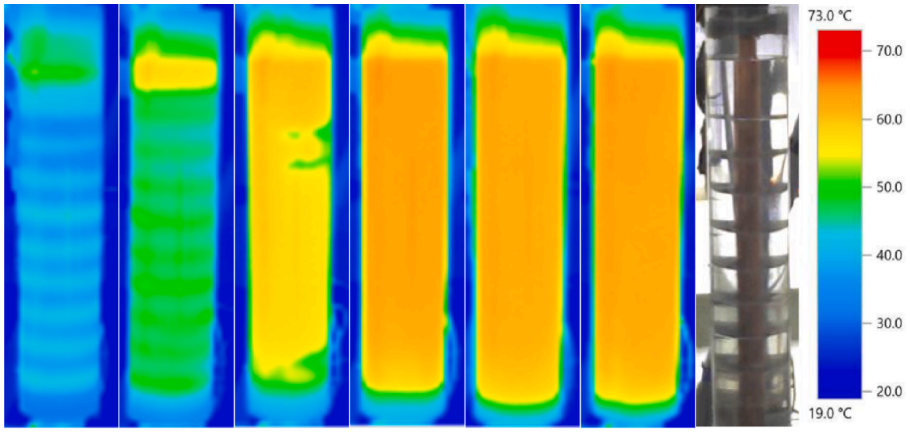
(i)



(a). 1h (b). 2 h (c). 3 h (d). 4h (e). 5 h (f). 6 h

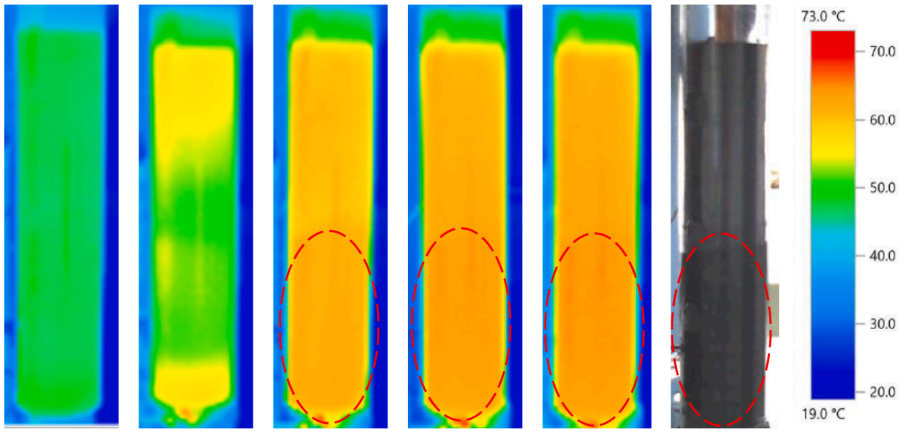
(ii)

Fig. 8. Dynamic temperature variation of PCM HX (i), PCM longitudinal fin HX (ii), PCM circular fin HX (iii), at 1,2,3,4,5 and 6 h and PCM EG HX (iv) and PCM/EG/fin HX (v) at 30, 60, 90, 120, and 150 min of charging an inlet temperature of HTF of 70℃ and 2.61 $l.min^{-1}$.



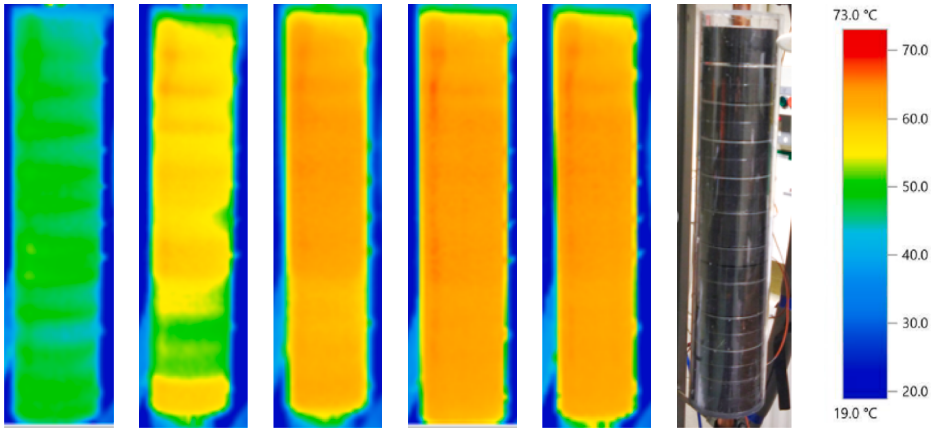
(a). 1h (b). 2h (c). 3h (d). 4h (e). 5h (f). 6h

(iii)



(a). 30 min (b). 60 min (c). 90 min (d). 120 min (e). 150 min

(iv)



(a). 30 min (b). 60 min (c). 90 min (d). 120 min (e). 150 min

(v)

Fig. 8. (*continued*).

PCM was above 56.8℃ after 3 h and by the end of 4 h of charging 90 % of the PCM had an average temperature above 61.3℃ with a thin solid layer of PCM below the first fin in the bottom zone. Conduction was the major mode of heat transfer during the initial period of charging in systems A, B, and C, then it became a combination of conduction and convection as the PCM started melting. Although, the temperature histories of the first three heat exchangers were not enough to track the melt front of the PCM, the thermal images provided better visualization of the melt front.

The thermal images of the PCM/EG HX as displayed in Fig. 8(iv). indicate faster charging rates than the previous systems. During the first 30 min of charging, the average PCM reached 47℃ and by the end of 90 min of charging more than 90 % of the PCM was above 61℃. The average PCM temperature rose to 63℃ after 120 min of charging. During the entire charging process conduction was the major mode of heat transfer as the PCM was embedded in the microporous sites of EG.

The thermal images of PCM/EG/fin HX are like that of PCM/EG HX with a much faster-charging response. This is evident from the thermal images in Fig. 8(iv)(b) and Fig. 8(v)(b). After 60 min of charging more than 80 % of the PCM in the PCM/EG/fin HX was above 57℃ whereas it was less than 50 % in PCM/EG HX. All the PCM had reached 63 ℃ in 90 min of charging. A combination of PCM/EG and aluminium fins presented a faster heat transfer response compared to all other systems evaluated. The combination of EG and circular fins provided more a uniform conductive heat transfer area which resulted in very high heat transfer rate.

3.2.3. Heat transfer characteristics

The Fig. 9. compares the average heat transfer rate over every five minutes of charging of the PCM HX, PCM longitudinal fin HX, PCM circular fin HX, PCM/EG HX and the PCM/EG/fin HX. For all the HXs the heat transfer rate is initially high during the initial period of charging due to the large temperature gradient between the inlet temperature of HTF and PCM layers around the tube. The dominant heat transfer mechanism during this stage is conduction, where heat is transferred through the solid PCM by direct molecular interactions. As the melting process progressed, the heat transfer rate continued to decrease and the temperature gradient diminished. Wang et al. [39] and Gasia et al. [9] have observed a similar trend during the charging process.

The dominant heat transfer mechanism during the initial stages of charging is conduction for the first three heat exchangers, where heat is transferred through the solid PCM by direct molecular interactions. As the process progresses, the melt front thickens and the conductive heat transfer drops. However, the reduction in conduction heat transfer is compensated by the establishment of natural convection within the growing liquid PCM layer. This convection flow helps maintain the heat transfer rate and prevents it from further decreasing. However, with the increase in PCM temperature, the effect of natural convection starts diminishing as it is confined to the lower part of the container and the upper part dominates by conduction heat transfer. Consequently, the overall heat transfer rate gradually decays as the remaining solid PCM continues to melt. Overall, the melting process involves a transition from conduction-dominated heat transfer to convection-dominated heat transfer, with the latter compensating for the decrease in conduction as the molten layer thickness increases. However, the PCM/EG HX and the PCM/EG/fin HX have conduction dominated heat transfer throughout the charging process. As the PCM is confined within the micro porous sites of EG, natural convection doesn't have any role in heat transfer. The extensive wide conductive network structure of the EG and the extended fin surface provide high heat transfer rate throughout the process. However, the heat transfer rate diminishes as the temperature gradient between the HTF and the PCM decreases.

As can be seen, the average charging power of PCM HX is much less compared to all the other systems due to its significantly low heat transfer area. This difference is more significant during the earlier stages of charging where the conduction dominates. The average charging power of the PCM HX, PCM longitudinal fin HX, and PCM circular fin HX during the conduction dominated heat transfer period was 122 W, 183 W and 265 W respectively. During the convection dominated charging period, their average heat transfer rate dropped to 34 W, 48 W and 58 W respectively. Then the average thermal power further dropped to 8 W, 7 W and 8 W respectively. Based on the thermal behaviour described, it can be inferred that the presence of fins improves the overall heat transfer rate during the melting process. However, their effectiveness is particularly pronounced during the early stage of melting when conduction is the dominant heat transfer mechanism.

Contrary to the first three cases PCM/EG HX and PCM/EG/fin HX showed a very strong charging power throughout the process. Kevin et al. [28] reported a similar result in their study. The average charging power of the system during the initial five minutes of charging was 630 W for PCM/EG HX and 690 W for PCM/EG/fin HX, which was 6 times higher than that of PCM HX, four times higher than longitudinal fin HX and three times higher than that of circular fin HX. From the Fig. 9. it can be deduced that most of the thermal energy during the charging process was transferred into the PCM in less than 70 min of charging in both systems with an average charging power of 70 W and 95 W, respectively during this period. During this period, the average charging power of the PCM/EG/fin HX was three times higher than that of PCM HX, two times higher than longitudinal fin HX and 1.6 times higher than that of circular fin HX. This clearly states the supremacy of EG/fin combination on the charging performance of the PCM heat exchanger system.

Fig. 10 compares the time averaged charging powers of PCM HX, PCM longitudinal fin HX, PCM circular fin HX, PCM/EG HX and PCM/EG/fin HX. Since the PCM mass is the same for all the systems (within 10 % variation) the time averaged charging power can be compared between all the given systems. The average charging power of the systems was calculated using equation (3). PCM HX system had the least charging power due to the lowest heat transfer area. The time averaged

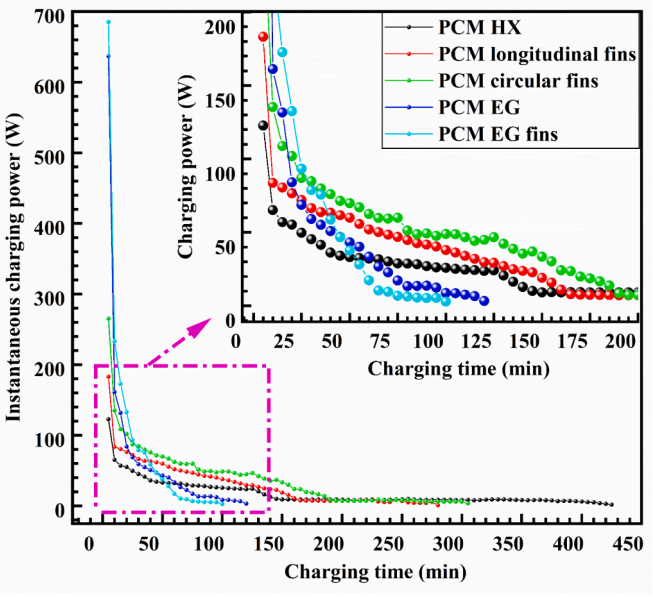


Fig. 9. Instantaneous heat transfer rate during charging of the PCM HX with various heat transfer enhancement methods.

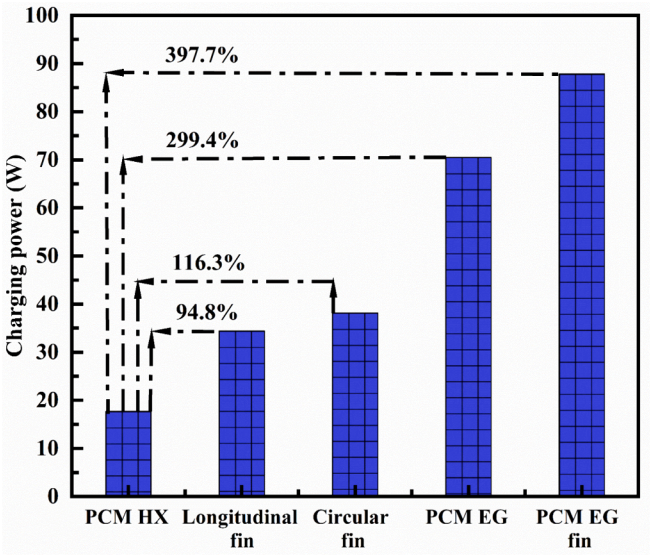


Fig. 10. Time averaged heat transfer rate during the charging period analysis of different HXs.

charging power was significantly enhanced by the addition of various heat transfer enhancement methods. As can be observed in Fig. 10. the time averaged heat transfer rate during the charging process of PCM longitudinal fin HX, PCM circular fin HX, PCM/EG HX and the PCM/EG/fin HX was 94.8 %, 116 %, 299 % and 397.7 % higher than that of PCM HX. As can be noticed, the charging power of circular fin configuration was slightly higher than that of the longitudinal fin. This was due to the sandwich heating effect of circular fins along with the mild natural convection. The addition of 25 wt% of EG resulted in 124 % increase in charging power compared to PCM longitudinal fin HX and 78 % increase compared to PCM circular fin HX. Medrano et al. [27] and Kevin et al. [28] reported high average thermal power of PCM/EG systems compared to finned systems in their studies. PCM/EG/fin HX had the highest average thermal power among the systems studied, which was 124 % higher than that of PCM circular fin HX and 25 % higher than PCM/EG HX. This is attributed to the high conductive network provided by the combination of EG and circular fins. This thermal behaviour was in conjunction with that of the instantaneous charging powers of the system.

Fig. 11 compares the variation of cumulative energy storage with time when charging with 70 ℃ hot water at 2.61 lmin^{-1}. Though the PCM content of the PCM HX was higher than the other HX configurations, the final value of thermal energy stored in the PCM HX is comparatively lower. This is because 20 % of the PCM at the bottom zone of the PCM HX is below 50 ℃ even after eight hours of charging, as can be seen in Fig. 7(a). Both PCM longitudinal fin HX and PCM circular fin HX exhibited the same trend of cumulative energy storage, with a slightly higher energy storage rate for circular fin configuration. The PCM/EG HX and PCM/EG/fin HX followed a similar trend in thermal energy stored during the initial period of charging, however, due to the higher charging power exhibited by the PCM/EG/fin HX, the cumulative energy stored curve starts deviating. overall, the trend of thermal energy stored was consistent with the variation of heat transfer rates.

Fig. 12 illustrates the charging period heat transfer enhancement ratio of PCM HX with the addition of various heat transfer enhancement methods. It can be deduced from the heat transfer enhancement ratio that the use of various heat transfer enhancement methods has a great influence on the heat transfer rates of PCM HX. Longitudinal fins have the advantage of an extended heat transfer area which augments natural convection. This resulted in 1.78 times faster melting rate than PCM HX. Whereas PCM circular fin HX exhibited more uniform heating due to

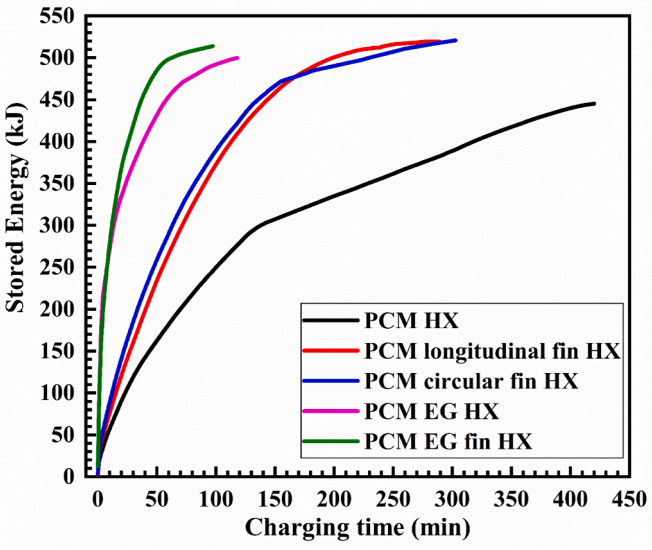


Fig. 11. Cumulative thermal energy stored in of various HX configuration investigated with time when the systems are charged with 70℃ hot waters at 2.61lmin^{-1}.

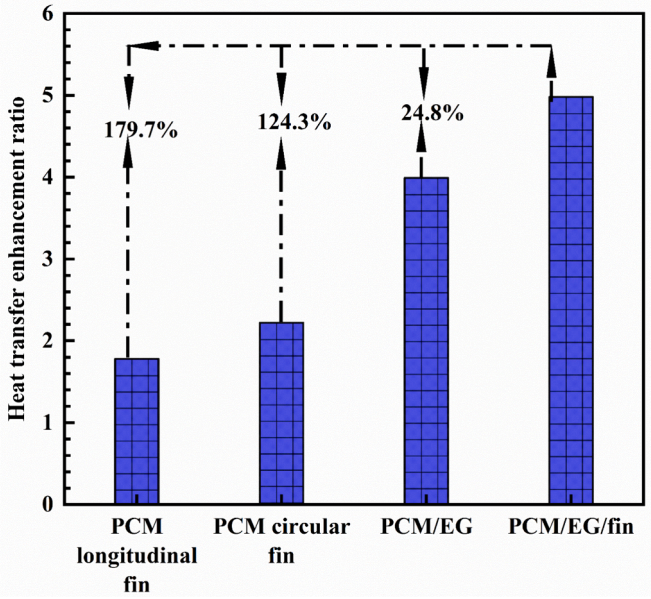


Fig. 12. Comparison of charging heat transfer enhancement of PCM HX with the addition of various heat transfer enhancement methods.

which resulted 2.22 times more heat transfer. PCM/EG composites system was much superior to the finned systems. The wide thermal conductive network structure of EG provided a high charging power and resulted in four times enhancement in charging rate. However, the combination of PCM/EG/fin was found to be highly effective and achieved 180 % higher enhancement than longitudinal fins, 124 % higher enhancement than circular fins and 25 % higher enhancement than the PCM/EG combination.

3.3. Discharging period analysis

3.3.1. Discharging characteristics

To assess the thermal performance of the LHTES units during the discharging period, the dynamic variation of the PCM at different locations of the systems of PCM HX, PCM longitudinal fin HX, PCM circular fin HX, PCM/EG HX and PCM/EG/fin HX was recorded and presented in Fig. 13. The systems were discharged using mains water at a flow rate of 2.6 l.min^{-1} and the trend of temperature variation of the PCM for two hours was observed. The HTF outlet temperature increases due to the high-temperature gradient between the HTF and the liquid PCM during the initial period of discharging, and a large drop in PCM temperature is observed as reported by Tiari et al. [37]. Since the HTF flows upwards through the pipe, the bottom zone temperature (T1-T3) shows a faster drop than the other sets of thermocouple readings. As the PCM in the bottom zone of PCM HX did not melt during the charging (T1-T4), this zone showed a comparatively slower temperature drop than the liquid zone as the PCM is in its sensible cooling region. The overall rate of temperature drop of PCM HX was the slowest of the systems studied. Whereas systems PCM longitudinal fin HX and PCM circular fin HX exhibited a clear phase transition region during discharging. Within 120 min, more than 50 % of the PCM in both systems was in a solidification process, indicating a higher discharging power compared to PCM HX. Unlike the charging process, all the temperature sensors of PCM longitudinal fin HX and PCM circular fin HX showed a uniform rate of temperature reduction, and temperature profiles of all the zones had a similar rate of temperature decrease throughout the discharging process. This is because the natural convection does not have as significant a role in the solidification process as observed by Fadl et al. [7] and Khan and Khan [21] where conduction plays the major role in discharging.

Like the charging profiles, high heat transfer rates, and uniform

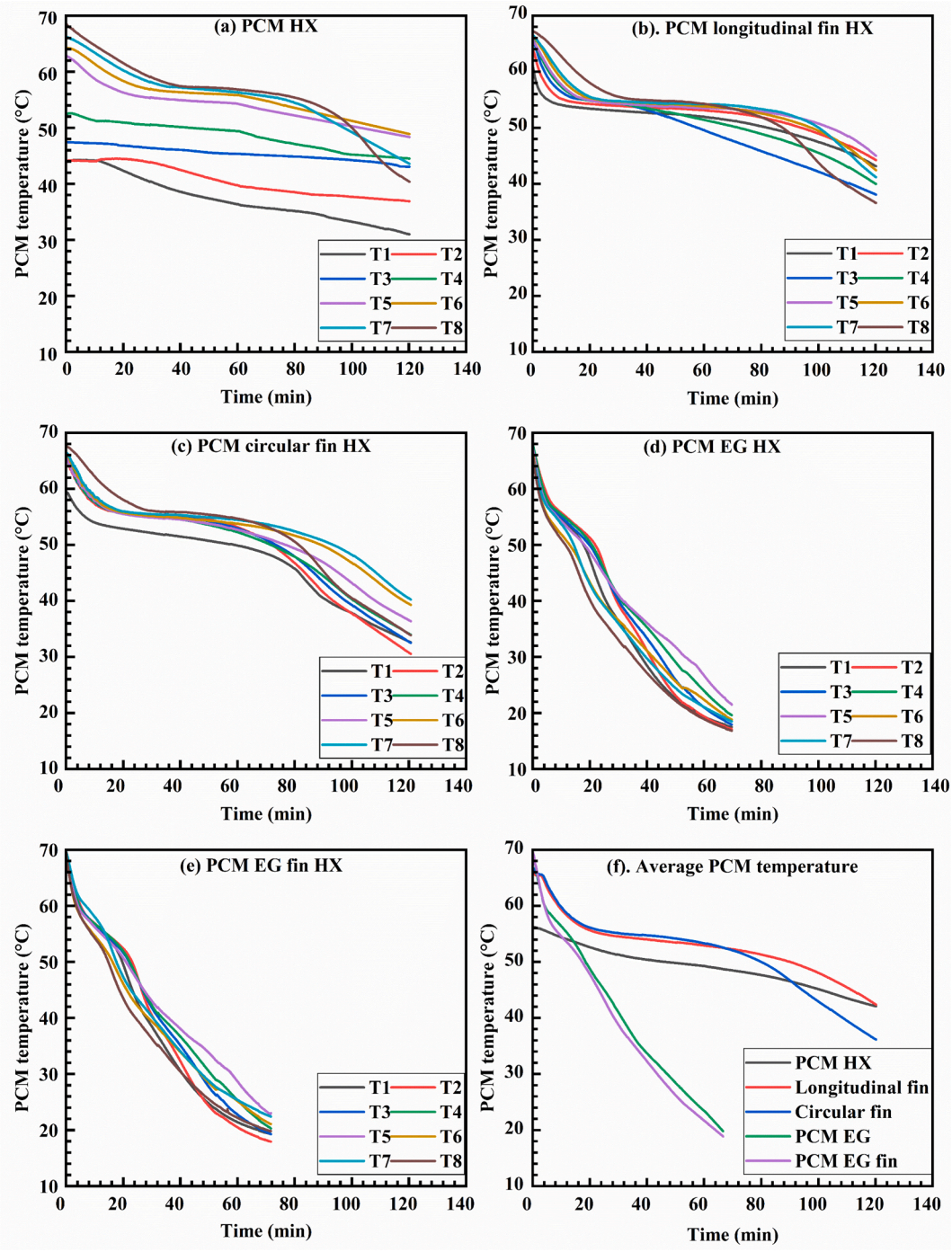


Fig. 13. Transient temperature distribution of PCM HX, PCM longitudinal fin HX, PCM circular fin HX, PCM/EG HX and PCM/EG/fin HX during discharging.

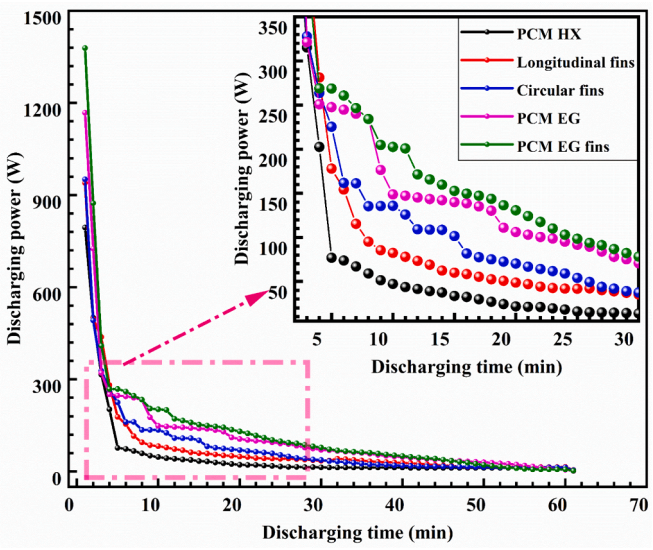


Fig. 14. The intensity of thermal energy discharged from the PCM systems every 5 min of discharging.

temperature drops were observed for PCM/EG HX and PCM/EG/fin HX. Both systems completed discharging in less than 70 min and temperature values in all the locations of thermocouple dropped to 20℃. As discussed before, the wide conductive network of EG resulted in a quick discharge response of the RT55/EG system. Since conduction is the major mode of heat transfer during discharging, the discharging rates of PCM/EG HX and PCM/EG/fin HX are very high as compared to the other systems studied. This is evident from the time required by the systems to reach 40℃ as shown by the average PCM temperature variation profiles in Fig. 13 (f).

3.3.2. *Heat transfer performances of the PCM HXs*

To investigate the effect of heat transfer enhancement methods on the discharging performance of PCM HX configuration, instantaneous discharging power of the systems in every one-minute interval is represented in Fig. 14. It can be observed that in all systems the discharging power during the first five minutes of discharging is very high compared to the rest of the process. This is due to the high-temperature gradient between the PCM and the HTF. As the cold HTF passes through the copper tube, the layer of PCM around the copper tube starts solidifying and imposes a high thermal resistance to the heat transfer. As the process progresses, the thickness of the solid PCM layer increases resulting in considerable drop-in heat transfer rate. Convection has role in heat transfer only during the initial period of the discharging process. As the solid PCM layer forms around the copper tube, heat transfer through conduction dominates. However, due to the low thermal conductivity of PCM, the overall heat transfer rate of the PCM HXs drops. Similar observations were made by Gasia et al. [9,10].

As can be observed, PCM HX had the lowest discharging power among the PCM HXs investigated throughout the process. However, it showed a comparatively high average heat transfer of 300 W during the initial five minutes and then dropped below 50 W. Then the system attained a constant low rate of discharging power during the rest of the process. A similar trend was observed for PCM longitudinal fin HX and PCM circular fin HX with an average discharging power of around 450 W during the first five minutes. During the initial period of discharging, the circular fin configuration exhibited slightly higher and uniform discharging power than PCM longitudinal fin HX. This was because, during discharging of PCM, natural convention doesn't have significant role, whereas conduction dominates throughout the process. However, after 30 min of discharging, both configurations continued to discharge at almost the same discharging powers. Both PCM/EG HX and PCM/EG/fin HX exhibited much higher discharging rates than the other configurations. It was consistent with the temperature history of the PCM. During the first five minutes of discharging the average discharging power of PCM/EG HX was 550 W and 640 W for PCM/EG/fin HX. More than 75 % of the thermal energy was discharged from PCM/EG and PCM/EG/fin HXs in 30 min of discharging. Whereas it was less than 45 % in other HXs. However, the discharging power diminished as the process continued due to the low temperature gradient between the HTF inlet

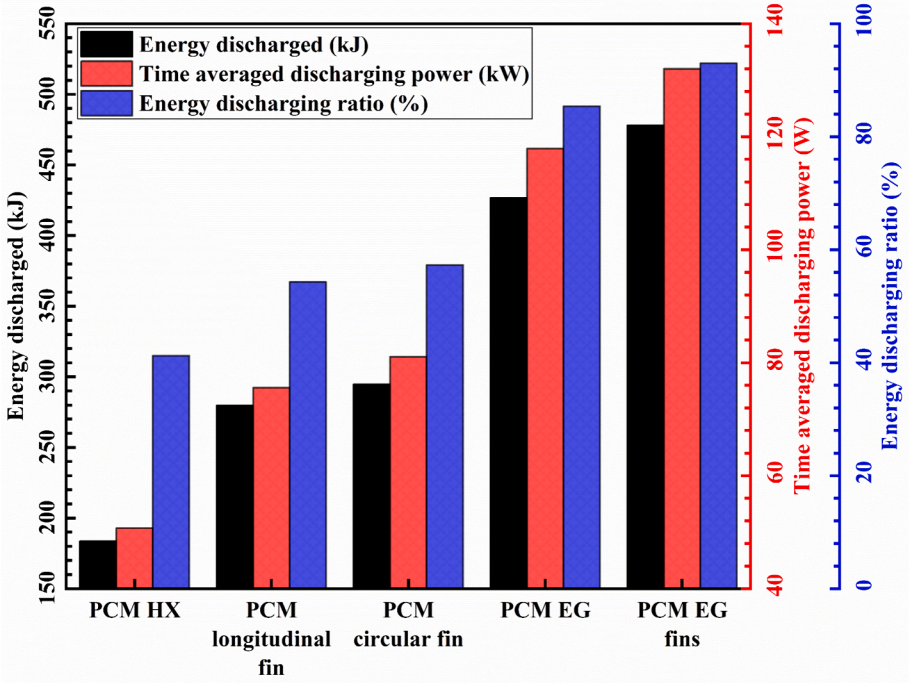


Fig. 15. Comparison of the different systems based on the thermal energy discharged, time averaged discharging power and energy discharging ratio based on one hour of discharging.

Table 4
Quantitative comparison of thermal energy discharged and time-averaged discharging power among different systems.

	Increase in thermal energy discharged (%)	Enhancement in time average discharging power (%)
PCM radial fin HX	52.3	49
PCM circular fin HX	60.5	60.9
PCM/EG HX	132.5	132.5
PCM/EG/fin HX	160.4	160.41

temperature and PCM.

In short, it can be concluded that the heat transfer enhancement methods like longitudinal fins and circular fins have a significant influence on the heat transfer rates at the beginning of the process, which decreases considerably as the discharging process continues. This was also reported by Gasia et al. [9]. However, PCM/EG HX and PCM/EG/fin presented significantly higher heat transfer rates over the other HX configurations throughout the discharging process. The effect of wide porous structure of the EG was high during the conduction dominated discharging period. The combination of EG and circular fin resulted in a higher heat transfer rate in PCM/EG/fin HX than the PCM/EG HX.

Fig. 15 compares the thermal energy discharged, time average discharging power and the energy discharging ratio over sixty minutes of discharging of the five HX configurations. As can be observed, all the heat transfer enhancement methods had significant effect on the discharging heat transfer performance of the PCM HX, due to the increase in heat transfer area. Table 4. quantitatively presents the effect of enhancement on the discharging period of PCM HX. 180 kJ of thermal energy was discharged from PCM HX in 60 min of discharging at an average discharging power of 50 W. Whereas the energy discharged increased by 52.3 % with the addition of longitudinal fins and 60.5 % with circular fins. In addition to that, the time averaged discharging power was 49 % higher in PCM longitudinal fin HX and 60.9 % higher in PCM circular fin HX compared to PCM HX. It can be inferred from these results that convection doesn't play much role in the energy discharged. Whereas the whole discharging process was conduction dominated. During charging, convective heat transfer was the major mode of heat transfer in PCM longitudinal fin HX and the convection was not that strong in PCM circular fin HX. Compared to PCM HX, 132.5 % more thermal energy was discharged from PCM/EG HX with 132 % higher average discharging power, and 160.4 % more energy was retrieved back from PCM/EG/fin HX with 160 % higher average discharging power. A similar trend can be observed in the energy discharging ratio, which is calculated using the equation (4). More than 90 % of the total energy transferred to the PCM/EG/fin HX was discharged in 60 min of discharging with mains water. It was more than 80 % in PCM/EG HX, 60 % in PCM longitudinal fin HX and PCM circular fin HX. PCM HX had the lowest energy discharging ratio. Very high values of energy discharged, the time average discharging power and the energy discharging ratio of PCM/EG/fin HX were attributed to the combined effect of EG network structure and circular fins. This emphasises the dominance of conduction in the discharging process.

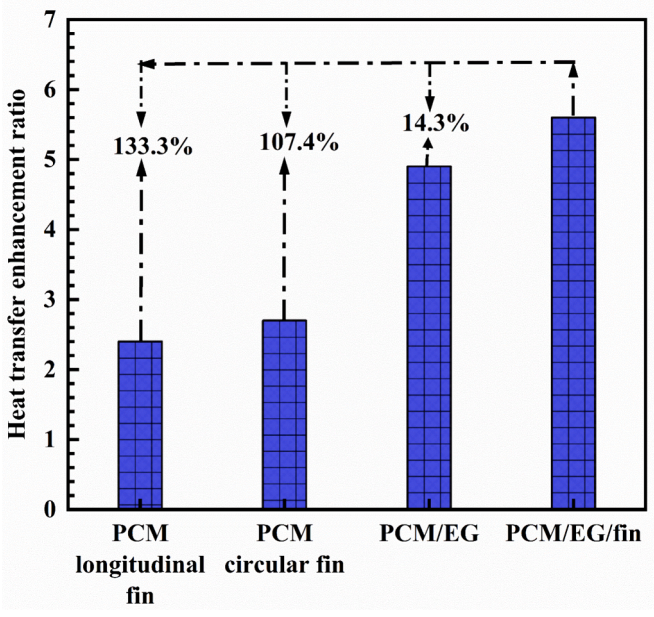


Fig. 16. Comparison of heat transfer enhancement of PCM HX with the addition of various heat transfer enhancement methods.

Fig. 16 illustrates the heat transfer enhancement with various HX configurations compared to the PCM HX during the discharging period. As can be seen, heat transfer enhancement with PCM/EG and PCM/EG/fin combinations are significantly higher than the fin configurations indicating the supremacy of EG composites over the fins during discharging process. This is attributed to the strong conductive network structure of the EG. The significant improvement in heat transfer observed with the PCM/EG/fin combination compared to other configurations can be attributed to the synergistic advantages offered by both the EG and fin components.

3.4. PCM leakage

The PCM/EG modules and the PCM/EG HX were analysed to study the leakage of molten PCM from the EG, when the composite is above the melting point of PCM. The Fig. 17. illustrates the physical condition of the PCM/EG modules and the TES fabricated with the PCM/25 wt% EG compressed disc after repeated charging and discharging cycles. To take the photographs and investigate the PCM/EG blocks for segregation, the outer container of the HX system was cut open. As can be observed in Fig. 17. (a)-(b), during the repeated thermal cycling test of the small sample of PCM/EG compressed module, the leakage of PCM was not severe. Even after repeated thermal cycling, there was no significant PCM leakage to make a difference in the weight of the compressed module. The liquid PCM around the PCM/EG module in the Fig. 17 (b) represents a negligible amount of PCM on the surface of the module. However, when the PCM/EG modules were arranged into a long vertical column in the TES units, considerable segregation of PCM and EG were observed. Fig. 17 (c)-(d) represents the physical condition of the PCM/EG HX after repeated charging and discharging cycles. 70 g of PCM was segregated from the PCM/EG composite disc after repeated three thermal cycles. It is evident that repeated thermal cycles affected the stability of PCM/EG compressed modules and resulted in considerable leakage of PCM from the EG. This is clearly visible in the Fig. 8 (iv) (c-d), where the colour changes in the thermal image at the bottom region of the system demonstrates accumulation of liquid PCM (represented in red dotted line). PCM/EG/fin HX in Fig. 17 (e-f) system also exhibited a segregation of PCM and EG, but with less intensity compared to PCM/EG HX. It can be deduced that, with the long column of PCM/EG compressed modules divided into sections with circular fins, this resulted in less segregation of PCM and EG in the PCM/EG/fin. However, the segregation of PCM and EG within the short columns was still observed, and this resulted in cracks on the compressed modules, as indicated in Fig. 17 (e-f).

4. Conclusion

The study aimed to investigate the effect of various heat transfer enhancement methods such as longitudinal fins, circular fins, PCM/EG composite, and a combination of EG-circular fins on the thermal performance of the PCM HX during both charging and discharging processes.

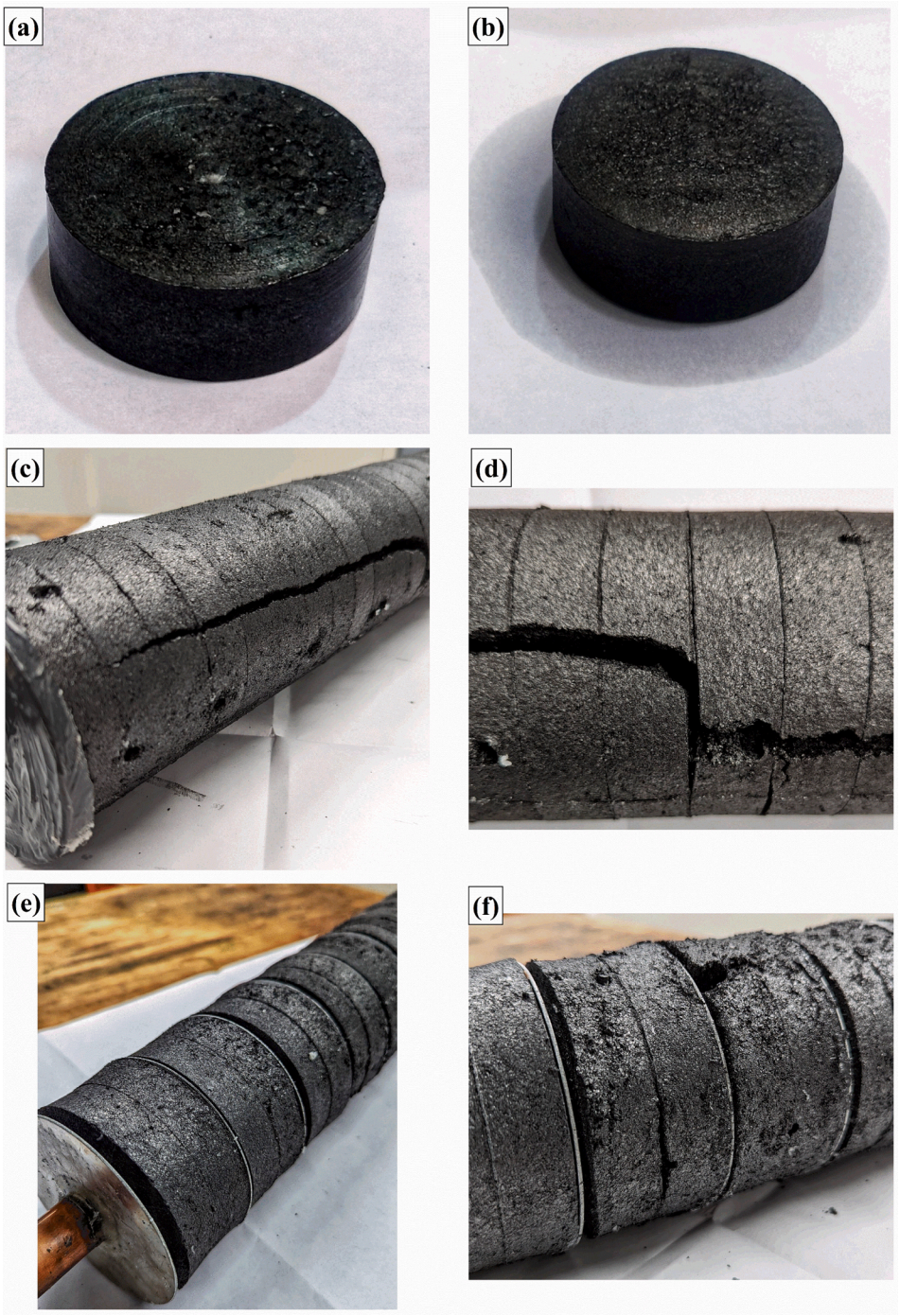


Fig. 17. Images of the PCM/EG composites before and after the thermal cycles (a),(b): (a) PCM/EG before leakage test, (b) PCM/EG composite module after repeated leakage testing, (c)-(d): (c) PCM/EG HX system after repeated charging and discharging cycles, (e)-(f) PCM/EG/fin HX system after repeated charging and discharging cycles.

- Without fins or with longitudinal fins, natural convection dominated heat transfer was observed during melting with significant temperature stratification. However, circular fins resulted in uniform temperature distribution in the PCM during both charging and discharging, with slightly higher heat transfer rate than longitudinal fins. Though, convection was the major mode of heat transfer during charging, discharging process was conduction dominated.
- Conduction dominated heat transfer rate was observed in the PCM/EG HX and PCM/EG/fin HX during both charging and discharging resulted in uniform temperature distribution. The wide conductive network provided by the combination of EG, and circular fin in the PCM/EG/fin HX resulted in best charging and discharging performance among the TES units compared. Besides, the overall discharging power of system with EG and circular fins was 12 % higher than that of the PCM/EG HX.
- Considerable segregation of liquid PCM and EG was observed in PCM/EG and PCM/EG/fin HX, which resulted in the formation of cracks and affected the stability of the compressed modules. This impact needs further research.
- These test results clearly demonstrate the combination of PCM/EG composite and fins can be employed in developing a high-power thermal energy storage unit that can be integrated with a heat

pump to utilise the surplus energy available in the grid for domestic hot water application. The uniform temperature distribution and high charging and discharging powers offered by this combination is highly beneficial to store the excess energy in short period of time and to maximise the discharged energy in the useful temperature range.

Further detailed studies are needed to enhance the compatibility between EG and PCM, enabling widespread use of EG as a heat transfer enhancer without the segregation of PCM. To address this issue, two potential approaches can be considered. Firstly, TES systems can be designed with macro encapsulation of the compressed PCM/EG modules, containing the leakage and segregation of liquid PCM from the EG in a small, confined space. Alternatively, chemical treatment can be applied to modify the microstructure of EG, enhancing its affinity towards PCM and mitigating the issue of segregation. Additional research in these areas is crucial to optimize the performance and practical implementation of PCM/EG systems, ensuring efficient heat transfer and the effective utilization of available energy sources.

CRediT authorship contribution statement

Ajay Muraleedharan Nair: Writing – original draft, Methodology, Investigation, Formal analysis, Conceptualization. **Christopher Wilson:** Writing – review & editing, Supervision, Resources, Methodology. **Babak Kamkari:** Writing – review & editing. **Jake Locke:** Resources. **Ming Jun Huang:** Writing – review & editing, Supervision. **Philip Griffiths:** Writing – review & editing, Supervision. **Neil J Hewitt:** Project administration, Funding acquisition.

Declaration of competing interest

The authors declare that they have no known competing financial interests or personal relationships that could have appeared to influence the work reported in this paper.

Data availability

The authors do not have permission to share data.

Acknowledgement

This study is a part of the SPIRE-2 project and the authors acknowledge the financial support from the European Union's INTERREG VA Programme (Grant Number IVA5038). The authors acknowledge the funding support from EPSRC/UKRI project LoT-NET (Grant number: EP/R045496/1). The authors extend their sincere gratitude to Roy Brelsford and Simon Hodge (Composite Lab, Mechanical Engineering) for providing all the technical support for fabricating the TES units.

References

[1] Agyenim F, Hewitt N, Eames P, Smyth M. A review of materials, heat transfer and phase change problem formulation for latent heat thermal energy storage systems (LHTESS). Renew Sustain Energy Rev 2010:615–28. https://doi.org/10.1016/j.rser.2009.10.015.
[2] Agyenim F, Eames P, Smyth M. A comparison of heat transfer enhancement in a medium temperature thermal energy storage heat exchanger using fins. Sol Energy 2009;83(9):1509–20. https://doi.org/10.1016/j.solener.2009.04.007.
[3] Arteconi A, Hewitt NJ, Polonara F. State of the art of thermal storage for demand-side management. Appl Energy 2012;93:371–89. https://doi.org/10.1016/j.apenergy.2011.12.045.
[4] Belessiotis GV, Papadokostaki KG, Favvas EP, Efthimiadou EK, Karellas S. Preparation and investigation of distinct and shape stable paraffin/SiO2 composite PCM nanospheres. Energ Conver Manage 2018;168:382–94. https://doi.org/10.1016/j.enconman.2018.04.059.
[5] Eames PC, Griffiths PW. Thermal behaviour of integrated solar collector/storage unit with 65 °C phase change material. Energ Conver Manage 2006;47(20):3611–8. https://doi.org/10.1016/j.enconman.2006.02.029.
[6] Egea, A. (2022) 'Experimental performance of a novel scraped surface heat exchanger for latent energy storage for domestic hot water generation', 193.
[7] Fadl M, Eames PC. An experimental investigation of the heat transfer and energy storage characteristics of a compact latent heat thermal energy storage system for domestic hot water applications. Energy 2019;188. https://doi.org/10.1016/j.energy.2019.116083.
[8] Fang Y, Qu ZG, Zhang JF, Xu HT, Qi GL. Charging performance of latent thermal energy storage system with microencapsulated phase-change material for domestic hot water. Energ Buildings 2020;224. https://doi.org/10.1016/j.enbuild.2020.110237.
[9] Gasia J, Diriken J, Bourke M, Van Bael J, Cabeza LF. Comparative study of the thermal performance of four different shell-and-tube heat exchangers used as latent heat thermal energy storage systems. Renew Energy 2017;114:934–44. https://doi.org/10.1016/j.renene.2017.07.114.
[10] Gasia J, Maldonado JM, Galati F, De Simone M, Cabeza LF. Experimental evaluation of the use of fins and metal wool as heat transfer enhancement techniques in a latent heat thermal energy storage system. Energ Conver Manage 2019;184:530–8. https://doi.org/10.1016/j.enconman.2019.01.085.
[11] Griffiths PW, Eames PC. Performance of chilled ceiling panels using phase change material slurries as the heat transport medium. Appl Therm Eng 2007;27(10):1756–60. https://doi.org/10.1016/j.applthermaleng.2006.07.009.
[12] Griffiths PW, Huang MJ, Smyth M. Improving the heat retention of integrated collector/storage solar water heaters using Phase Change Materials Slurries. Int J Ambient Energy 2007;28(2):89–98. https://doi.org/10.1080/01430750.2007.9675029.
[13] He Z, Ma H, Lu S. Design and experimental investigation of topology-optimized fin structures for enhanced heat transfer in latent heat thermal energy storage units. J Storage Mater 2024;80. https://doi.org/10.1016/j.est.2023.110272.
[14] Huang MJ, Eames PC, McCormack S, Griffiths P, Hewitt NJ. Microencapsulated phase change slurries for thermal energy storage in a residential solar energy system. Renew Energy 2011;36(11):2932–9. https://doi.org/10.1016/j.renene.2011.04.004.
[15] Huang P, Wei G, Cui L, Xu C, Du X. Experimental and numerical optimization of cascaded PCM heat sink by using low melting point alloys. Energ Conver Manage 2022;269. https://doi.org/10.1016/j.enconman.2022.116149.
[16] Ibrahim NI, Al-Sulaiman FA, Rahman S, Yilbas BS, Sahin AZ. Heat transfer enhancement of phase change materials for thermal energy storage applications: A critical review. *Renew Sustain Energy Rev* Elsevier Ltd 2017:26–50. https://doi.org/10.1016/j.rser.2017.01.169.
[17] Jiang ZY, Qu ZG. Lithium–ion battery thermal management using heat pipe and phase change material during discharge–charge cycle: A comprehensive numerical study. Appl Energy 2019;242. https://doi.org/10.1016/j.apenergy.2019.03.043.
[18] Jun Huang M. The effect of using two PCMs on the thermal regulation performance of BIPV systems. Sol Energy Mater Sol Cells 2011;95(3):957–63. https://doi.org/10.1016/j.solmat.2010.11.032.
[19] Kalapala L, Devanuri JK. Influence of operational and design parameters on the performance of a PCM based heat exchanger for thermal energy storage – A review. *J Storage Mater* Elsevier Ltd 2018:497–519. https://doi.org/10.1016/j.est.2018.10.024.
[20] Karami R, Kamkari B. Experimental investigation of the effect of perforated fins on thermal performance enhancement of vertical shell and tube latent heat energy storage systems. Energ Conver Manage 2020;210. https://doi.org/10.1016/j.enconman.2020.112679.
[21] Khan Z, Khan ZA. An experimental investigation of discharge/solidification cycle of paraffin in novel shell and tube with longitudinal fins based latent heat storage system. Energ Conver Manage 2017;154:157–67. https://doi.org/10.1016/j.enconman.2017.10.051.
[22] Khan Z, Khan ZA. Experimental investigations of charging/melting cycles of paraffin in a novel shell and tube with longitudinal fins based heat storage design solution for domestic and industrial applications. Appl Energy 2017;206:1158–68. https://doi.org/10.1016/j.apenergy.2017.10.043.
[23] Khan, Zakir, Khan, Zulfiqar and Ghafoor, A. (2016) 'A review of performance enhancement of PCM based latent heat storage system within the context of materials, thermal stability and compatibility', *Energy Conversion and Management*. Elsevier Ltd, pp. 132–158. doi:10.1016/j.enconman.2016.02.045.
[24] Khan Z, Khan Z, Tabeshf K. Parametric investigations to enhance thermal performance of paraffin through a novel geometrical configuration of shell and tube latent thermal storage system. Energ Conver Manage 2016;127:355–65. https://doi.org/10.1016/j.enconman.2016.09.030.
[25] Li C, Zhao X, Chen J. Diversiform microstructure silicon carbides stabilized stearic acid as composite phase change materials. Sol Energy 2020;201. https://doi.org/10.1016/j.solener.2020.02.102.
[26] Lin W, Ling Z, Zhang Z, Fang X. Experimental and numerical investigation of sebacic acid/expanded graphite composite phase change material in a double-spiral coiled heat exchanger. J Storage Mater 2020;32. https://doi.org/10.1016/j.est.2020.101849.
[27] Medrano M, Yilmaz MO, Nogués M, Martorell I, Roca J, Cabeza LF. Experimental evaluation of commercial heat exchangers for use as PCM thermal storage systems. Appl Energy 2009;86(10):2047–55. https://doi.org/10.1016/j.apenergy.2009.01.014.
[28] Merlin K, Delaunay D, Soto J, Traonvouez L. Heat transfer enhancement in latent heat thermal storage systems: Comparative study of different solutions and thermal contact investigation between the exchanger and the PCM. Appl Energy 2016;166:107–16. https://doi.org/10.1016/j.apenergy.2016.01.012.
[29] Murray RE, Groulx D. Experimental study of the phase change and energy characteristics inside a cylindrical latent heat energy storage system: Part 1

consecutive charging and discharging. Renew Energy 2014;62:571–81. https://doi.org/10.1016/j.renene.2013.08.007.
[30] Nair, A.M., Wilson, C., Huang, M.J., Griffiths, P. and Hewitt, N. (2022) 'Phase change materials in building integrated space heating and domestic hot water applications: A review', 54(March). doi:doi.org/10.1016/j.est.2022.105227.
[31] Sadeghi G, Mehrali M, Shahi M, Brem G, Amirhoushang M. Experimental analysis of Shape-Stabilized PCM applied to a Direct-Absorption evacuated tube solar collector exploiting sodium acetate trihydrate and graphite. Energ Conver Manage 2022;269. https://doi.org/10.1016/j.enconman.2022.116176.
[32] Safari V, Kamkari B, Hewitt N, Hooman K. Experimental comparative study on thermal performance of latent heat storage tanks with pin, perforated, and rectangular fins at different orientations. Thermal Science and Engineering Progress 2024;48. https://doi.org/10.1016/j.tsep.2024.102401.
[33] Sari A, Karaipekli A. Thermal conductivity and latent heat thermal energy storage characteristics of paraffin/expanded graphite composite as phase change material. Appl Therm Eng 2007;27(8–9):1271–7. https://doi.org/10.1016/j.applthermaleng.2006.11.004.
[34] Sari A, Karaipekli A. Preparation, thermal properties and thermal reliability of palmitic acid/expanded graphite composite as form-stable PCM for thermal energy storage. Sol Energy Mater Sol Cells 2009;93(5):571–6. https://doi.org/10.1016/j.solmat.2008.11.057.
[35] Shank K, Bernat J, Justice Q, Niksiar P, Tiari S. Experimental study of a latent heat thermal energy storage system assisted by variable-length radial fins. J Storage Mater 2023;68. https://doi.org/10.1016/j.est.2023.107692.
[36] Soliman AS, Fouda MS, Cheng P. Power saving in a central air conditioning system by using multiple PCMs integrated with fresh air path. Energ Buildings 2023;300. https://doi.org/10.1016/j.enbuild.2023.113691.
[37] Tiari S, Mahdavi M, Qiu S. Experimental study of a latent heat thermal energy storage system assisted by a heat pipe network. Energ Conver Manage 2017;153:362–73. https://doi.org/10.1016/j.enconman.2017.10.019.
[38] Wang W, Yang X, Fang Y, Ding J, Yan J. Preparation and thermal properties of polyethylene glycol/expanded graphite blends for energy storage. Appl Energy 2009;86(9):1479–83. https://doi.org/10.1016/j.apenergy.2008.12.004.
[39] Wang Y, Yu K, Ling X. Experimental study on thermal performance of a mobilized thermal energy storage system: A case study of hydrated salt latent heat storage. Energ Buildings 2020;210. https://doi.org/10.1016/j.enbuild.2019.109744.
[40] Wu J, Feng Y, Liu C, Li H. Heat transfer characteristics of an expanded graphite/paraffin PCM-heat exchanger used in an instantaneous heat pump water heater. Appl Therm Eng 2018;142:644–55. https://doi.org/10.1016/j.applthermaleng.2018.06.087.
[41] Wu S, Li TX, Yan T, Dai YJ, Wang RZ. High performance form-stable expanded graphite/stearic acid composite phase change material for modular thermal energy storage. Int J Heat Mass Transf 2016;102:733–44. https://doi.org/10.1016/j.ijheatmasstransfer.2016.06.066.
[42] Xu T, Li Y, Chen J, Wu H, Zhou X, Zhang Z. Improving thermal management of electronic apparatus with paraffin (PA)/expanded graphite (EG)/graphene (GN) composite material. Appl Therm Eng 2018;140:13–22. https://doi.org/10.1016/j.applthermaleng.2018.05.060.
[43] Yang ZL, Walvekar R, Wong WP, Sharma RK, Dharaskar S, Khalid M. Advances in phase change materials, heat transfer enhancement techniques, and their applications in thermal energy storage: A comprehensive review. J Storage Mater 2024. https://doi.org/10.1016/j.est.2024.111329.
[44] Yazici MY, Saglam M, Aydin O, Avci M. Thermal energy storage performance of PCM/graphite matrix composite in a tube-in-shell geometry. Thermal Science and Engineering Progress 2021;23. https://doi.org/10.1016/j.tsep.2021.100915.
[45] Zhang S, Wu W, Wang S. Experimental investigations of Alum/expanded graphite composite phase change material for thermal energy storage and its compatibility with metals. Energy 2018;161:508–16. https://doi.org/10.1016/j.energy.2018.07.075.
[46] Zheng R, Zhou H, Li C, Li J. Synergistic phase change and heat conduction of low melting-point alloy microparticle additives in expanded graphite shape-stabilized organic phase change materials. Chem Eng J 2024;482. https://doi.org/10.1016/j.cej.2024.149009.
[47] Zheng S, Li S, Dai R, Wei M, Tian R, Song P. Experimental study of thermal performance in a rectangular finned-tube latent heat storage device with composite polyethylene wax/expanded graphite. Case Studies in Thermal Engineering 2023;49. https://doi.org/10.1016/j.csite.2023.103388.
[48] Zhu Y, Yu Y, Qiu Y. (2021) 'Effect of fins with unequal length on the performance of cylindrical latent heat storage system'. J Storage Mater 2020;35. https://doi.org/10.1016/j.est.2020.102224.